LEP W measurements

Takayuki Saeki

International Center for Elementary Particle Physics (ICEPP),
University of Tokyo, 7-3-1 Hongo, Bunkyo-ku Tokyo, 113-0033, Japan

In June 1996, the LEP center-of-mass energy was raised to 161 GeV, just above the threshold of pair-production of W bosons, and LEP2 experiments started. ALEPH, DELPHI, L3, and OPAL experiments observed the pair-production of W bosons for the first time in e^+e^- collisions. Since then, the four experiments had been collecting data successfully at the energies of 161 – 209 GeV, and the data acquisition of LEP experiments was finished on 2nd November 2001. The total integrated luminosities amounted to about 710 pb^{-1} per each experiment and about 46 k W-pair events were produced in total. In this article, the results on W physics in LEP2 are presented, which cover the total cross section of the W boson pair-production, the W decay branching fractions, the triple gauge-boson couplings and the mass of the W boson. All the results are consistent with the Standard Model expectations within the measurement errors.

1   Introduction

In June 1996, the LEP2 started with the center-of-mass energy (CME) of 161 GeV, just above the threshold of pair-production of W bosons and LEP2 experiments started. This allowed us to observe and study the first W-pair production events through the four experiments, i.e. ALEPH, DELPHI, L3 and OPAL, in clean environment of e^+e^- collisions. Detailed descriptions of the four detectors can be found elsewhere [1,2,3,4]. On 2nd November 2001, the data acquisition of LEP experiments was finished. The recorded data through the LEP2 period corresponds to an integrated luminosities of about 710 pb^{-1} per experiment. The number of W-pair productions in LEP2 amounted to 11.5 k events per experiment, i.e. 46 k W-pair events in total. This article presents main results on W-pair production obtained by the four experiments using these data, covering the total cross section of the W boson pair-production, the W decay branching fractions, the triple gauge-boson couplings, and the mass of the W boson.

2   Selection

WW events are produced through three doubly resonant diagrams (s-channel γ and Z^0 exchange and t-channel ν exchange), called "CC03 diagrams", where each W can decay into quark pair or lepton-neutrino pair. This leads to the classification of WW events into three channels, i.e. fully hadronic, semileptonic, and fully leptonic channels. WW events are selected with good efficiency and high purity in the analyses, utilising corresponding event-topology to the three channels.
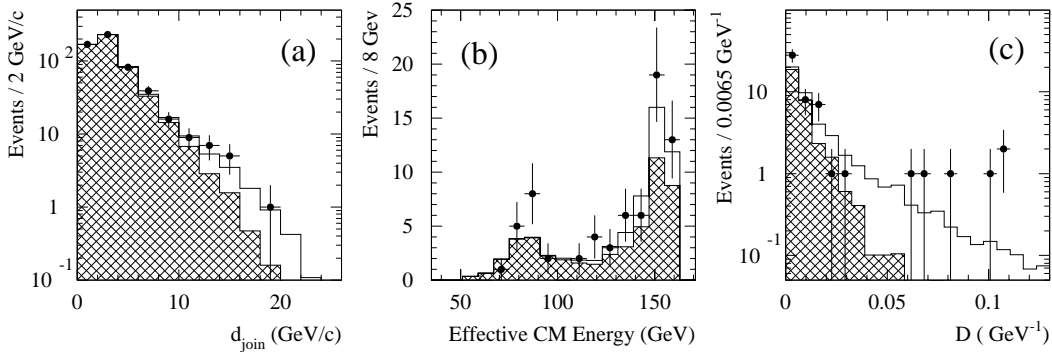
Figure 1: Selection for fully hadronic final state from DELPHI: comparison of data (points) with background (hatched-area) and WW signal (white area). (a) Differential 3-jet rate as function of d_{join}; (b) effective CME for events with at least 4 jets; (c) D variable for 4-jet events with effective CME > 115 GeV.

2.1 Fully hadronic channel

The typical final state of the fully hadronic events is specified by four hadronic jets whose energy sum is consistent with the center-of-mass energy. Display for a typical fully hadronic WW event from OPAL is shown in Figure 2, where four jets can be seen clearly. The event selection criteria were optimised in order to ensure that the final state was purely hadronic and in order to reduce the residual background. The background is dominated by electron-positron annihilation to $q\bar{q}(\gamma)$, with a cross section about two orders of magnitude larger than that for signal at 161 GeV.

Here the selection criteria for DELPHI experiment at 161 GeV is described. For each event, all particles are clustered into jets using the LUCLUS algorithm [5] with $d_{join} = 6.5$ GeV/c. At least 4 jets are required, with at least four particles in each jet. Figure 1 (a) shows the distributions of the differential 3-jet rate as a function of d_{join} for data and simulated WW and background events. Events coming from the radiative return Z peak are rejected by requiring the effective center-of-mass energy of e^+e^- annihilation to be larger than 115 GeV. The effective energy was estimated from the momentum of the radiative photon. Figure 1 (b) shows the distributions of the effective energy for events with at least 4 jets. Events are then forced into a 4-jet configuration, and a kinematically constrained fit performed, imposing energy and momentum conservation. The final cut is made on the variable

$$D = \frac{E_{min}\theta_{min}}{E_{max}(E_{max} - E_{min})}, \qquad (1)$$

where E_{min}, E_{max} are the energies of the jets with least and greatest energy, and θ_{min} is the smallest inter-jet angle, after the constrained fit. D is required to exceed 0.013 GeV^{-1} and discriminates well between the signal and the $q\bar{q}(\gamma)$ background. Figure 1 (c) shows the distributions of D variable after the other two cuts described above. The selection efficiency was computed from a sample of WW Monte Carlo events, and found to be $(61.3 \pm 2.0)\%$.

At 172 GeV, the ratio of the signal cross section to the cross section of Z^0/γ events is about four times larger than at threshold. Therefore, in the higher energies, some of the cuts are allowed to be relaxed and also improve the efficiency of the selections. Other selection cuts are rescaled in accordance with the increase in total energy. The selection efficiency of DELPHI was estimated to be $(82.7 \pm 1.6)\%$ at 172 GeV from Monte Carlo simulation. The residual cross sections of $q\bar{q}(\gamma)$ events after these selection procedures at 161 and 172 GeV were estimated to be 0.58 and 1.96 pb, respectively.

L3

M_{jj} = 74.1 GeV/c²

$M_{e\nu}$ = 85.0 GeV/c²

Jet 2

Jet 1   electron 37.8 GeV

July 11, 1996 06:42am

First W pair event observed by the L3 Experiment at LEP 2.

$e^+ e^- \rightarrow W^+ W^-$
$\quad \hookrightarrow e^- \bar{\nu}$
$\quad \hookrightarrow$ jet + jet

Applying energy and momentum conservation to the event shows that the two jets and the electron-neutrino originate from the decay of two W bosons.
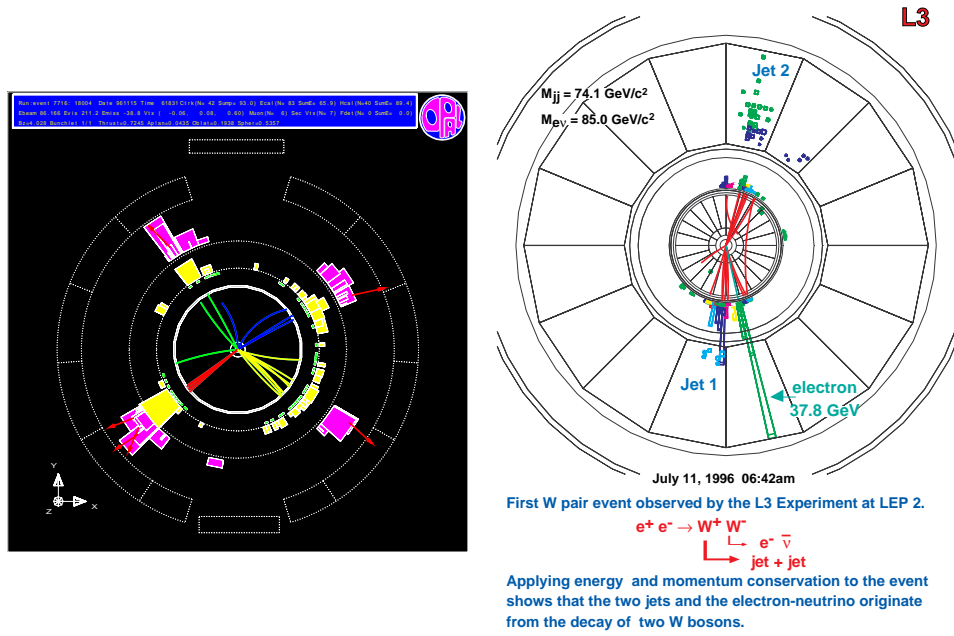
Figure 2: Left-hand side: event display of typical fully hadronic WW event from OPAL. Right-hand side: event display of typical semileptonic WW event from L3.

From 189 GeV, DELPHI adopted a neural network for selections of the fully hadronic final state. A feed forward neural network is used to improve the selection quality of the signal from the 2-fermion (mainly $q\overline{q}(\gamma)$ events) and 4-fermion (mainly ZZ events) background. Input variables are different jet or event observables. The samples for training and testing the feed forward net consist of PYTHIA MC and real data. The overall selection efficiency was improved to be $(90.2 \pm 0.9)\%$. The cross section for the expected total background was estimated from simulation to be (2.06 ± 0.10) pb. The main contribution of background comes from $q\overline{q}(\gamma)$ events with gluon radiation.

2.2   Semileptonic channel

Semileptonic final states, $W^+W^- \rightarrow q\overline{q}\, l\overline{\nu}_l$, are expected to comprise 44% of W^+W^- decays. $W^+W^- \rightarrow q\overline{q}e\overline{\nu}_e$ and $W^+W^- \rightarrow q\overline{q}\mu\overline{\nu}_\mu$ events are characterised by two well-separated hadronic jets, a high momentum lepton and sizable missing momentum due to the unobserved neutrino. Display for a typical semileptonic WW event from L3 is shown in Figure 2, where two jets and one track for electron are seen. The signature for $W^+W^- \rightarrow q\overline{q}\tau\overline{\nu}_\tau$ events is two well separated jets from the hadronic W decay and one low multiplicity jet typically consisting of one or three tracks. The expected missing momentum is less well defined due to the additional neutrino(s) from the decay of the tau.

The selection criteria of $W^+W^- \rightarrow q\overline{q}\, l\overline{\nu}_l$ channel for OPAL experiment at 172 and 189 GeV are described here. The $W^+W^- \rightarrow q\overline{q}\, l\overline{\nu}_l$ event selection consists of three separate selections, one for each type of semileptonic decay. The $W^+W^- \rightarrow q\overline{q}\tau\overline{\nu}_\tau$ selection is applied only to events which fail the $W^+W^- \rightarrow q\overline{q}e\overline{\nu}_e$ and $W^+W^- \rightarrow q\overline{q}\mu\overline{\nu}_\mu$ selections.

At 172 GeV, each selection proceeds in four stages. Stage 1 is the identification of the candidate lepton. The track with the highest probability of being a lepton from either the decay $W \rightarrow e\overline{\nu}_e$ or $W \rightarrow \mu\overline{\nu}_\mu$ is identified. The $W^+W^- \rightarrow q\overline{q}\tau\overline{\nu}_\tau$ selection uses the track (or tracks) most consistent with being from a tau decay from $W^+W^- \rightarrow q\overline{q}\tau\overline{\nu}_\tau$. Stage 2 is the preselection. Cuts are applied to the data to reduce the background from $Z^0/\gamma \rightarrow q\overline{q}$ events. Stage 3 is the relative likelihood selection which, based on kinematic variables and the lepton candidate,

are used to distinguish signal events ($W^+W^- \to q\overline{q}e\overline{\nu}_e$ $W^+W^- \to q\overline{q}\mu\overline{\nu}_\mu$ and $W^+W^- \to q\overline{q}\tau\overline{\nu}_\tau$) from $Z^0/\gamma \to q\overline{q}$ background events. Events passing the likelihood selection are considered to be $W^+W^- \to q\overline{q}l\overline{\nu}_l$ candidates. Stage 4 is the event categorisation. Having suppressed the background using the relative likelihood selection, a second relative likelihood is applied to the $W^+W^- \to q\overline{q}e\overline{\nu}_e$ and $W^+W^- \to q\overline{q}\mu\overline{\nu}_\mu$ candidates in order to categorise them as either $W^+W^- \to q\overline{q}e\overline{\nu}_e$, $W^+W^- \to q\overline{q}\mu\overline{\nu}_\mu$ or $W^+W^- \to q\overline{q}\tau\overline{\nu}_\tau$ events.

Table 1: OPAL selection efficiencies for the different $W^+W^- \to q\overline{q}l\overline{\nu}_l$ channels after event categorisation showing the cross contamination in each selection at 172 GeV. The efficiencies have been corrected for differences between data and Monte Carlo. The errors include both statistical and systematic uncertainties.

	Generated as		
	$W^+W^- \to q\overline{q}e\overline{\nu}_e$	$W^+W^- \to q\overline{q}\mu\overline{\nu}_\mu$	$W^+W^- \to q\overline{q}\tau\overline{\nu}_\tau$
Selected as			
$W^+W^- \to q\overline{q}e\overline{\nu}_e$	$85.1 \pm 0.9\%$	$0.1 \pm 0.1\%$	$3.9 \pm 0.3\%$
$W^+W^- \to q\overline{q}\mu\overline{\nu}_\mu$	$0.2 \pm 0.1\%$	$87.6 \pm 0.8\%$	$4.4 \pm 0.3\%$
$W^+W^- \to q\overline{q}\tau\overline{\nu}_\tau$	$4.7 \pm 0.5\%$	$5.2 \pm 0.5\%$	$61.4 \pm 1.2\%$

Table 1 shows the efficiencies of the selections for $W^+W^- \to q\overline{q}l\overline{\nu}_l$ events after categorisation into the different channels at 172 GeV. These efficiencies include corrections which account for observed differences between the data and the Monte Carlo simulation. The uncertainties include both systematic and statistical contributions. Efficiency corrections and systematic errors arising from discrepancies between data and Monte Carlo simulation were determined by studying data and Monte Carlo "mixed events" formed by superposing LEP1 hadronic Z^0 decay events and single hemispheres from LEP1 events identified as Z^0 decays to charged lepton pairs.

At 189 GeV, the selection consists of five stages, which can be summarized as

- a loose preselection to remove events with low multiplicity or little visible energy;

- identification of the observed track in the event most consistent with being the leptonic decay or a W boson;

- separate likelihood selection for $W^+W^- \to q\overline{q}e\overline{\nu}_e$ $W^+W^- \to q\overline{q}\mu\overline{\nu}_\mu$ and $W^+W^- \to q\overline{q}\tau\overline{\nu}_\tau$;

- re-classification of $W^+W^- \to q\overline{q}\tau\overline{\nu}_\tau$ events which are identified by the $W^+W^- \to q\overline{q}e\overline{\nu}_e$ and $W^+W^- \to q\overline{q}\mu\overline{\nu}_\mu$ selections;

- rejection of 4-fermion background;

The first three stages are optimized for the rejection of the $e^+e^- \to q\overline{q}$ background which has an expected cross section about six times larger than the W-pair production cross section at 189 GeV. The $W^+W^- \to q\overline{q}l\overline{\nu}_l$ likelihood selection have a significant efficiency for other 4-fermion events e.g. single W and qqll events. For this reason additional cuts are applied to events passing the likelihood selection to reduce backgrounds from these processes.

The 4-fermion background rejection consists of three separate parts. Firstly, cuts are applied to reject qqll events for $W^+W^- \to q\overline{q}e\overline{\nu}_e$ and $W^+W^- \to q\overline{q}\mu\overline{\nu}_\mu$ selections. Secondly, the $W^+W^- \to q\overline{q}\tau\overline{\nu}_\tau$ selection accepts approximately 40% of hadronically decaying single W events ($q\overline{q}e\overline{\nu}_e$) where the electron is beyond the experimental acceptance. An additional likelihood selection is applied for these events. Finally, Ze^+e^- final state background, where one electron is beyond the experimental acceptance, is reduced for $W^+W^- \to q\overline{q}e\overline{\nu}_e$ selection with two kinematic fits, the first using signal hypothesis and the second using Ze^+e^- background hypothesis.
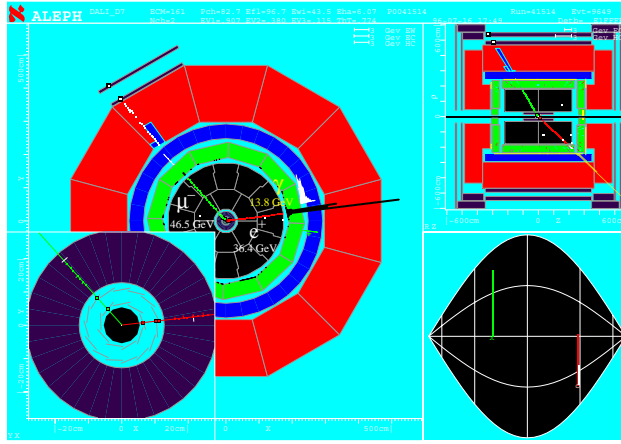
Figure 3: Event display of typical fully leptonic WW event from ALEPH.

In addition to the likelihood selection, cut based selections are used to identify $W^+W^-\rightarrow q\overline{q}e\overline{\nu}_e$ and $W^+W^-\rightarrow q\overline{q}\mu\overline{\nu}_\mu$ events where the lepton track is either poorly reconstructed or is beyond the tracking acceptance, but with clear evidence of an electron or muon in the calorimeter or muon chambers. These additional selections improve the overall efficiency by approximately 3 % (5 %) for $W^+W^-\rightarrow q\overline{q}e\overline{\nu}_e$ ($W^+W^-\rightarrow q\overline{q}\mu\overline{\nu}_\mu$) events.

Table 2 shows the efficiencies of the selections for $W^+W^-\rightarrow q\overline{q}\,l\overline{\nu}_l$ events after categorisation into the different channels at 189 GeV. One can see improvements in all channels being compared with Table 1.

Table 2: OPAL selection efficiencies for the different $W^+W^-\rightarrow q\overline{q}\,l\overline{\nu}_l$ channels after event categorisation showing the cross contamination in each selection at 189 GeV.

	Generated as		
	$W^+W^-\rightarrow q\overline{q}e\overline{\nu}_e$	$W^+W^-\rightarrow q\overline{q}\mu\overline{\nu}_\mu$	$W^+W^-\rightarrow q\overline{q}\tau\overline{\nu}_\tau$
Selected as			
$W^+W^-\rightarrow q\overline{q}e\overline{\nu}_e$	85.4%	0.1%	3.8%
$W^+W^-\rightarrow q\overline{q}\mu\overline{\nu}_\mu$	0.1%	89.2%	4.3%
$W^+W^-\rightarrow q\overline{q}\tau\overline{\nu}_\tau$	4.5%	4.4%	68.4%

2.3 Fully leptonic channel

The typical fully leptonic WW events consist of two acoplanar energetic leptons with significant missing energy in detectors. Display for a typical fully leptonic event from ALEPH is shown in Figure 3, where two tracks for positron and muon can be seen. ALEPH developed two selections for the $W^+W^-\rightarrow l^+\nu l^-\overline{\nu}$ signal ($l = $ e, μ or τ) for the threshold measurement. The two selections have overall efficiencies (62.7% and 66.9%) and background levels (0.038 pb and 0.028 pb) at 161 GeV. They have similar efficiencies and background levels, but differ in their sensitivities to the individual di-lepton channels. The first analysis is based on topological information and is sensitive to all channels, where events are accepted if they contain two or four charged tracks with zero total electric charge. The second analysis requires from two to six charged tracks and the presence of at least one high momentum electron or muon. This leads to a comparatively lower efficiency (24% instead of 48%) for events where both W's decay to tau, but the efficiency is higher in all other channels. Both analyses apply photon vetoes against radiative di-lepton events. Events are accepted as WW candidates if they pass either of the two selections and the

combined efficiency is 74% for a background of 0.053 pb. The two selections are also used in the analysis at 172 GeV without significant changes. They have the overall efficiencies (65% and 69%) and background levels (0.035 pb and 0.058 pb) at this energy, and the combined efficiency is 74% for a background of 0.065 pb. The residual background is dominated by $\gamma\gamma \to \tau\tau$ and non-CC03 4-fermion events at both energies. The largest detector related systematic effects come from the photon vetoes, with a systematic uncertainty of $\pm2\%$. The overall systematic errors amount to ±0.029 at 161 GeV and ±0.07 at 172 GeV, and are dominated by Monte Carlo statistics.

Similar selections are applied at higher energies. At 189 GeV, the inclusive combination of the two selections has an overall efficiency of $62.2 \pm 0.4\%$ when combined assuming lepton universality. Table 3 shows the selection efficiencies of ALEPH for the different $l^+\nu l^-\overline{\nu}$ channels after event categorisation showing the cross contamination in each selection at 189 GeV.

Table 3: ALEPH selection efficiencies for the different $l^+\nu l^-\overline{\nu}$ channels after event categorisation showing the cross contamination in each selection at 189 GeV.

	Generated as					
	$e\nu e\nu$	$e\nu\mu\nu$	$e\nu\tau\nu$	$\mu\nu\mu\nu$	$\mu\nu\tau\nu$	$\tau\nu\tau\nu$
Selected as						
$e\nu e\nu$	57.8%	––	8.8%	––	––	0.5%
$e\nu\mu\nu$	––	59.0%	4.7%	––	4.6%	0.3%
$e\nu\tau\nu$	3.0%	4.2%	50.1%	––	0.3%	4.3%
$\mu\nu\mu\nu$	––	––	––	61.9%	8.3%	0.3%
$\mu\nu\tau\nu$	––	4.2%	0.3%	3.5%	52.9%	3.5%
$\tau\nu\tau\nu$	0.2%	0.4%	7.7%	0.4%	6.0%	36.5%

2.4 Number of W-pair events

The numbers of WW events selected for each channel by four experiments at 161/172/183/189 GeV are shown in Table 4. We collected 117/467/3248/12654 WW candidates at 161/172/183/189 GeV, respectively, in total of four experiments. Table 5 shows approximate numbers of WW events produced in e^+e^- collisions in LEP2 in each year. The total number of WW events produced in the LEP2 period amounted to about 11.5 k events per each experiment and about 46 k events in total of four experiments.

Table 4: The numbers of WW candidates selected for each channel by four experiments at 161/172/183/189 GeV. (N.B.: ALEPH adopted a high-efficiency and low-purity selection in 4q channel at 189 GeV, and the number of WW candidates in 4q channel in ALEPH is larger than the other experiments.)

	$W^+W^- \to q\overline{q}q\overline{q}$	$W^+W^- \to q\overline{q}\,l\overline{\nu}_l$	$W^+W^- \to l^+\nu l^-\overline{\nu}$	Total
ALEPH	16/65/423/3438	16/44/326/1106	6/10/60/220	38/119/809/4764
DELPHI	15/65/391/1340	12/45/288/906	2/8/59/188	29/118/738/2434
L3	9/61/473/1514	11/40/297/1035	2/9/54/186	22/110/824/2735
OPAL	14/57/438/1435	12/55/361/1066	2/8/78/220	28/120/877/2721
Total	54/248/1725/7727	51/184/1272/4113	12/35/251/814	117/467/3248/12654

Table 5: Number of WW events produced in e^+e^- collisions in LEP2.

Year	CME (GeV)	σ_{WW}(pb)	Int. lumi. (1/pb) /exp	N_{WW} /exp
1996	161	3.4	11	0.04k
	172	11.9	10	0.1k
1997	183	15.4	~ 60	~ 0.9k
1998	189	16.3	~ 190	~ 3.1k
1999	$192 - 202$	~ 17	~ 220	~ 3.7k
2000	$202 - 209$	~ 17	~ 220	~ 3.7k
Total	$-$	$-$	~ 710	~ 11.5k

3 Determination of W-pair cross section

The $\mathrm{W}^+\mathrm{W}^-$ production cross section is measured by using likelihood method. For example, OPAL used the information from ten separate channels for these measurements. For each channel i, the probability of obtaining the number of observed events is calculated as a function of the $\mathrm{W}^+\mathrm{W}^-$ cross section, σ_{WW}, and the W branching fractions, using Poisson statistics and assuming Standard Model branching ratios. The likelihood $\mathcal{L}$ is formed from the product of these Poisson probabilities $\mathcal{P}_i$, of observing N_i events for a Monte Carlo prediction of μ_i events:

$$\mathcal{L} = \prod_i \mathcal{P}_i(N_i, \mu_i) = \prod_i \frac{\mu_i^{N_i} \exp(-\mu_i)}{N_i!}. \tag{2}$$

If μ_i is given as a function of σ_{WW}, the maximum likelihood value yields the measurement of the CC03 cross section.

Figure 4 shows the combined LEP W-pair cross section as a function of the CME. Also shown is the Standard Model predictions from YFSWW [6] and RACOONWW [7] (solid line), and for comparison, the cross sections if the ZWW coupling does not exist (dotted line) and if only the t-channel ν_e exchange diagram exists (dashed line). One can see the data points are consistent with the Standard Model prediction. Furthermore, the experimental points can be compared with the theoretical calculations from YFSWW and RACOONWW between 155 and 215 GeV for $M_{\mathrm{W}} = 80.35$ GeV. The two codes have been extensively compared and agree at a level better than 0.5 % at the LEP2 energies [8]. The calculations above 170 GeV, based for the two programs on the so-called leading pole (LPA) or double pole approximations (DPA) [9], have theoretical uncertainties decreasing from 0.7 % at 170 GeV to about 0.4 % at CME larger than 200 GeV, while in the threshold region a large theoretical uncertainty of 2 % is assigned [10]. This theoretical uncertainty is represented by a band in Figure 4. An error of 50 MeV on the W mass would translate into additional errors of 0.1 % (3.0 %) on the cross section predictions at 200 GeV (161 GeV, respectively). All results, up to the highest CME, are in agreement with the two theoretical predictions considered.

The agreement between the measured W-pair cross section, σ_{meas}^{WW}, and its expectations according to a given theoretical model, σ_{theo}^{WW}, can be expressed quantitatively in terms of their ratio, $R_{WW} = \sigma_{meas}^{WW}/\sigma_{theo}^{WW}$, averaged over the measurements performed by the four experiments at different energies in the LEP2 region. The above procedure has been used to compare the measurements at the eight energies between 183 and 207 GeV to the predictions of GENTLE[11], KORALW[12], YFSWW [6] and RACOONWW [7]. The measurements at 161 and 172 GeV have not been used in the combination because they were performed using data samples of low statistics and because of the high sensitivity of the cross section to the value of the W mass at these energies.
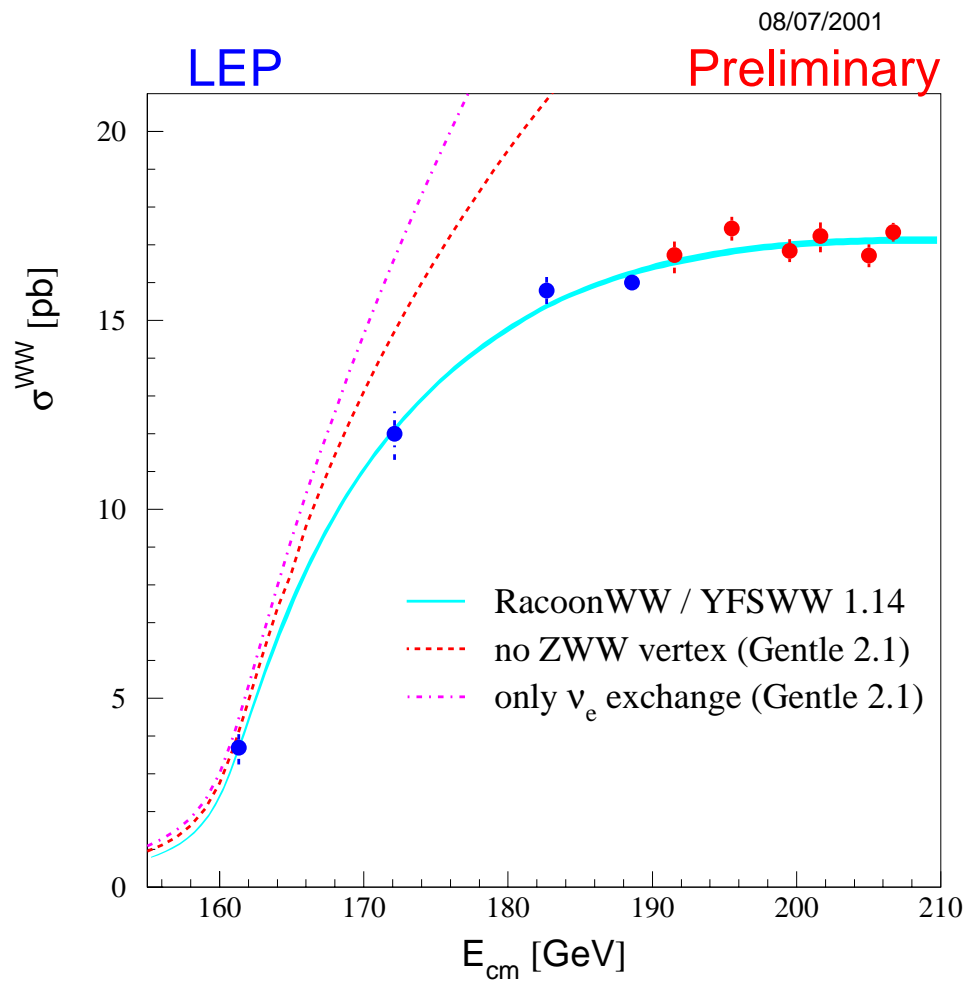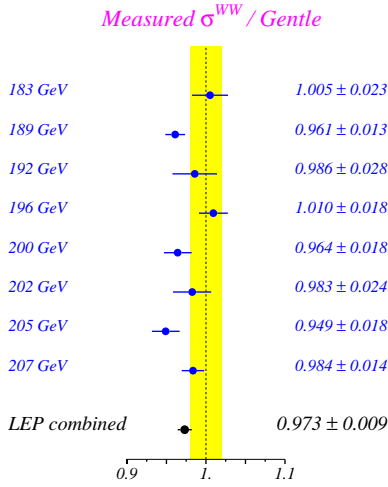
Figure 4: The W-pair cross section as a function of the CME. The data points are the LEP averages. Also shown is the Standard Model prediction (solid line), and for comparison, the cross sections if the ZWW coupling did not exist (dotted line) and if only the t-channel ν_e exchange diagram existed (dashed line).
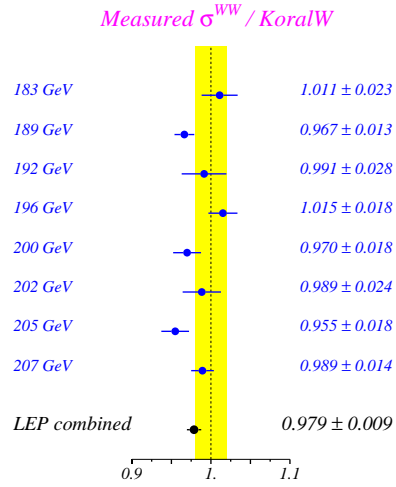
Measured σ^{WW} / Gentle

Measured σ^{WW} / KoralW

183 GeV		1.005 ± 0.023	
189 GeV		0.961 ± 0.013	
192 GeV		0.986 ± 0.028	
196 GeV		1.010 ± 0.018	
200 GeV		0.964 ± 0.018	
202 GeV		0.983 ± 0.024	
205 GeV		0.949 ± 0.018	
207 GeV		0.984 ± 0.014	
LEP combined		0.973 ± 0.009	

0.9   1.   1.1

183 GeV		1.011 ± 0.023	
189 GeV		0.967 ± 0.013	
192 GeV		0.991 ± 0.028	
196 GeV		1.015 ± 0.018	
200 GeV		0.970 ± 0.018	
202 GeV		0.989 ± 0.024	
205 GeV		0.955 ± 0.018	
207 GeV		0.989 ± 0.014	
LEP combined		0.979 ± 0.009	

0.9   1.   1.1

LEP WW Working Group Summer 2001

LEP WW Working Group Summer 2001

Figure 5: Comparison of predicted WW cross sections of GENTLE (left) and KORALW (right) with LEP2 measured cross section.

The combination of the ratio R_{WW} is performed using as input from the four experiments the 32 cross sections measured at each of the eight energies. For each model considered, these are converted into 32 ratios by dividing them by the corresponding theoretical predictions. The full 32×32 covariance matrix for the ratios is built taking into account the same sources of systematic errors used for the combination of the W-pair cross sections at these energies. The small statistical errors on the theoretical predictions at the various energies, taken as fully correlated for the four experiments and uncorrelated between different energies, are also translated into errors on the individual measurements of R_{WW}.

For each of the four models considered, two fits are performed: in the first, eight values of R_{WW} at the different energies are extracted, averaged over the four experiments: in the second, only one value of R_{WW} is determined, representing the global agreement of measured and predicted cross sections over the whole energy range.

The results of the two fits to R_{WW} for each of the four models considered are given in Figure 5 and 6. As already qualitatively noted from Figure 4, the LEP measurements of the W-pair cross section above threshold are in very good agreement to the predictions of YFSWW and RACOONWW. In contrast, the prediction from GENTLE and KORALW are more than 2 % too high with respect to the measurements. The main difference between these two sets of predictions come from non-leading $O(\alpha)$ electroweak radiative corrections to the W-pair production process, which are included (in the LPA/DPA approximation [9]) in both YFSWW and RACOONWW, but not in GENTLE and KORALW. Especially interesting is the comparison between KORALW and YFSWW, as the numerical results provided by the authors for KORALW are actually those of a downgraded version of YFSWW, such that the only difference between the two calculations are the screening of Coulomb interactions according to the prescription of Reference [13] and the inclusion of the non-leading $O(\alpha)$ electroweak radiative corrections to W-pair production (mainly radiation off W bosons and pure weak corrections). Of these two effects, only the latter is found to be relevant to the measurement of R_{WW}, while the former has a negligible impact on the total W-pair cross section [14].
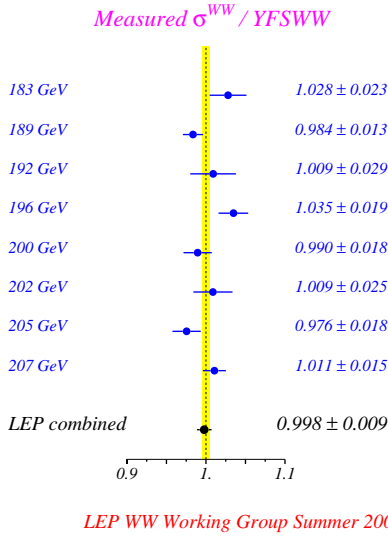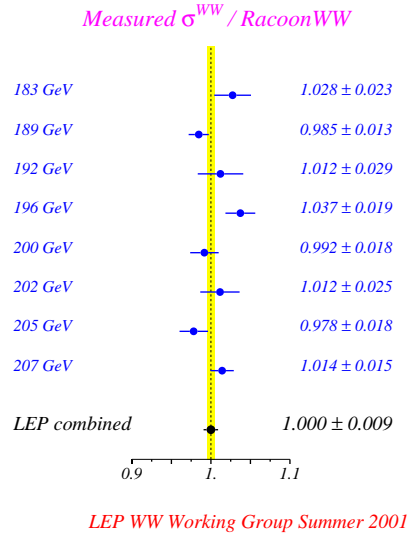
Figure 6: Comparison of predicted WW cross sections of YFSWW (left) and RACOONWW (right) with LEP2 measured cross section.

4 W branching fraction and CKM-matrix element V_{CS}

If μ_i is the function of a W branching fraction in equation 2, the maximum likelihood value yields the measurement of the corresponding W branching fraction, with and without the assumption of lepton universality. The results from each experiment are given in Table 6 and Figure 7, together with the result for the LEP combination.

The two combinations performed, with and without the assumption of lepton universality, both use as inputs from each of the four experiments the three leptonic branching fractions, with their systematic and observed statistical errors and their three by three correlation matrices. In the fit with lepton universality, the branching fraction to hadron is determined from that to leptons by constraining the sum to unity. In building the full 12×12 covariance matrix, it is assumed that the 4-jet QCD background components of the systematic error are fully correlated between different experiments both for the same and for different leptonic channels, as they arise mainly from the uncertainty on the WW cross section in the channel where both W bosons decay to hadrons. The combination procedure is consistent with that used for the combination of the total W-pair cross sections and outlined in the previous section, as the same sources of inter-experiment correlations are considered, while inter-energy correlations of systematic errors are taken into account internally by each experiment when deriving their average branching ratios.

Assuming lepton universality, the measured hadronic branching fraction is 67.92±0.17 (stat.) ±0.21 (syst.)% and the leptonic one is 10.69 ± 0.06 (stat.) ±0.07 (syst.)%. These results are consistent with their Standard Model expectations of 67.51% and 10.83% respectively [15].

Within the Standard Model, the branching fractions of the W boson depend on the six matrix elements $|V_{ij}|$ of the Cabibbo-Kobayashi-Maskawa (CKM) quark mixing matrix not involving the top quark [16]. Concerning measurements on CKM matrix elements by other experiments, apart from the elements describing the decays of the heavy top quark, the value of the element relating the quarks of the second generation is known with poorest precision. The $|V_{\mathrm{CS}}|$ is measured to be 1.04 ± 0.16 in semileptonic decays of D mesons [17] and $0.97 \pm 0.09(\mathrm{stat.}) \pm 0.07(\mathrm{syst.})$ in

Table 6: Summary of leptonic and hadronic W branching fractions.

Experiment	Lepton Non-universality			Lepton Universality
	$\mathrm{Br}(\mathrm{W}\rightarrow e\overline{\nu}_e)$ [%]	$\mathrm{Br}(\mathrm{W}\rightarrow\mu\overline{\nu}_\mu)$ [%]	$\mathrm{Br}(\mathrm{W}\rightarrow\tau\overline{\nu}_\tau)$ [%]	$\mathrm{Br}(\mathrm{W}\rightarrow q\overline{q})$ [%]
ALEPH	10.95 ± 0.31	11.11 ± 0.29	10.57 ± 0.38	67.33 ± 0.47
DELPHI	10.36 ± 0.34	10.62 ± 0.28	10.99 ± 0.47	68.10 ± 0.52
L3	10.40 ± 0.30	9.72 ± 0.31	11.78 ± 0.43	68.34 ± 0.52
OPAL	10.40 ± 0.35	10.61 ± 0.35	11.18 ± 0.48	67.91 ± 0.61
LEP	10.54 ± 0.17	10.54 ± 0.16	11.09 ± 0.22	67.92 ± 0.27
χ^2/d.o.f	14.9/9			18.8/11
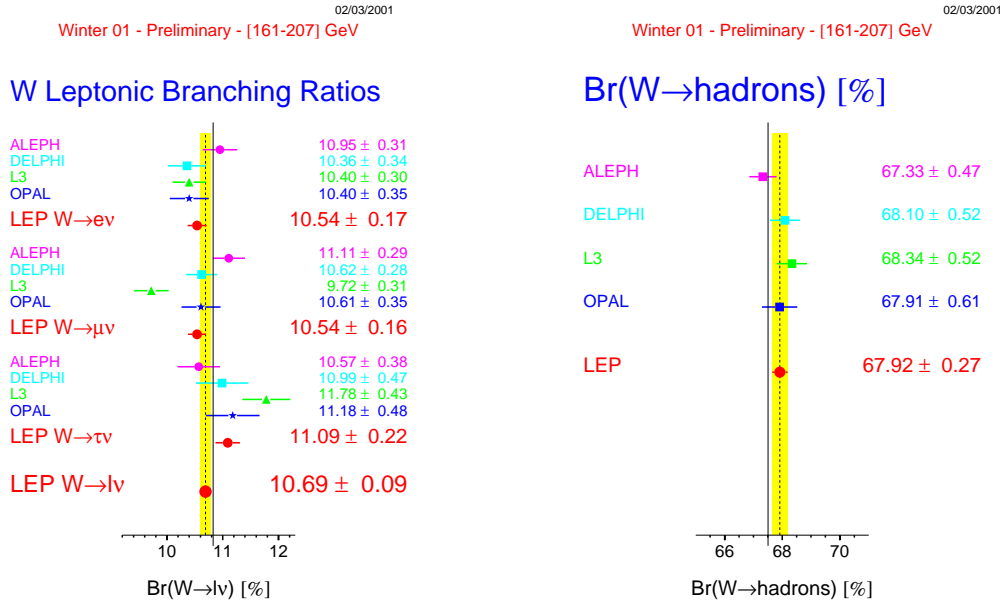
Figure 7: The results of measurements on WW branching fraction to lepton (left) and WW branching fraction to hadron (right). Each error on the measured values is the quadratic sum of statistical and systematic uncertainties.

charmed-tagged W decays [18].

In terms of the matrix elements, $|V_{ij}|$, the hadronic branching fraction of the W boson Br(W→qq̄) is given by

$$\frac{\text{Br(W} \to \text{q}\overline{\text{q}})}{1 - \text{Br(W} \to \text{q}\overline{\text{q}})} = \left(1 + \frac{\alpha_s(M_W)}{\pi}\right) \sum_{i=\text{u,c}; \, j=\text{d,s,b}} |V_{ij}|^2, \tag{3}$$

where $\alpha_s(M_W)$ is taken to be 0.121 ± 0.002. The LEP combined result for the branching fraction Br(W→qq̄) obtained from the fit assuming lepton universality gives:

$$\sum_{i=\text{u,c}; \, j=\text{d,s,b}} |V_{ij}|^2 = 2.039 \pm 0.025(Br(\text{W} \to \text{q}\overline{\text{q}})) \pm 0.0001(\alpha_s). \tag{4}$$

where the first error is due to the uncertainty on the branching fraction measurement and the second to the uncertainty on α_s. Using the experimental knowledge[17] of the sum, $|V_{ud}|^2 + |V_{us}|^2 + |V_{ub}|^2 + |V_{cd}|^2 + |V_{cb}|^2 = 1.0477 \pm 0.0074$, the above result can be interpreted as a measurement on $|V_{cs}|$, which is the least well determined of these elements:

$$|V_{cs}| = 0.996 \pm 0.013. \tag{5}$$

The error includes a ± 0.0006 contribution from the uncertainty on α_s and a ± 0.004 contribution from the uncertainties on the other CKM matrix elements, the largest of which is that on $|V_{cd}|$. These contributions are negligible in the error on this determination of $|V_{cs}|$, which is dominated by the ± 0.013 experimental error from the measurement of the W branching fractions.

5 Triple guage-boson couplings

The W$^+$W$^-$ production process involves the triple gauge-boson vertices between the W$^+$W$^-$ and the Z^0 or photon. All evidence for the existence of triple gauge-boson vertices and measurements of the Triple Gauge-boson Couplings (TGC's) had been indirect or was based on estimate from high energy pp̄ collisions [19] before LEP2. The measurement of these Triple Gauge-boson Couplings (TGC's) and the search for possible anomalous values in the very clean environment of e$^+$e$^-$ collisions is one of the principal physics goals at LEP2.

The most general Lorentz invariant Lagrangian [20,21,22,23,24] which describes the triple guage-boson interaction has up to fourteen independent terms, seven describing the WWγ vertex and seven describing the WWZ vertex. This parameter space is very large, and it is not currently possible to measure all fourteen couplings independently. Assuming electro-magnetic gauge invariance and C and P conservation the number of parameters reduces to five, which we can write as g_1^Z, κ_Z, κ_γ, λ_Z and λ_γ following the notation used in [20,21]. In the Standard Model $g_1^Z = \kappa_Z = \kappa_\gamma = 1$ and $\lambda_Z = \lambda_\gamma = 0$.

The TGC's contribute, via loop corrections, to observables which can be measured at LEP1 and there has been a rich discussion on the bounds in the parameter space that can be deduced from the huge amount of LEP1 precision data [25,26]. To parameterise the so-called "blind directions" in the multidimensional space of TGC's where the constraints from LEP1 analyses are very weak, three linear combination of these couplings have been proposed [20,21,22]. The three TGC's, $\alpha_{W\phi}$, α_W, and $\alpha_{B\phi}$, introduced to parametrise these linear combinations form the most general set of TGC's which can be embedded into an theory that preserve local SU(2)$_L \times$ U(1)$_Y$ invariance. In terms of the notation in [20] they are

$$\begin{aligned}
\alpha_{W\phi} &= \Delta g_1^Z \cos^2 \theta_w \\
\alpha_W &= \lambda_\gamma \\
\alpha_{B\phi} &= \Delta \kappa_\gamma - \Delta g_1^Z \cos^2 \theta_w
\end{aligned} \tag{6}$$

along with constraints $\Delta\kappa_Z = \Delta g_1^Z - \Delta\kappa_\gamma \tan^2\theta_w$ and $\lambda_\gamma = \lambda_Z$. The Δ denotes the deviations of the respective quantity from its non-zero Standard Model value and θ_w is the weak mixing angle. In the main analyses of four experiments, the couplings, $\Delta\kappa_\gamma$, Δg_1^Z and λ_γ are measured individually assuming the two other couplings to be fixed at zero, their Standard Model expectation.

5.1 Experimental variables

The important kinematic quantities for TGC measurements in W^+W^- events are the five variables:

- $\cos\Theta_W$, the production polar angle of the W^- boson.

- $\cos\theta^*_{-,+}$, the polar decay angle of the charged lepton or down type quark with respect to the flight direction of the $W^{-,+}$, measured in its rest frame.

- $\phi^*_{-,+}$, the azimuthal decay angle of the the charged lepton or down type quark with respect to the plane defined by the direction of $W^{-,+}$ and the incoming electron.

The total cross section of W-pair production is sensitive to the TGC's, but the differential cross section:

$$d\sigma = d\sigma(\Omega) \tag{7}$$
$$\Omega = (\Theta_W, \theta^*_{-,+}, \phi^*_{-,+}) \tag{8}$$

contains more pieces of information on TGC's. As a first step to extract the information on TGC's from $\sigma(\Omega)$, the momenta and energies of the decay products from W bosons are measured and fed into the kinematic fits which improve the resolution of the measurements of the five variables. For semileptonic events the charge of the reconstructed lepton together with the two jets determines the W^- direction and hence allows for unambiguous determination of the primary variable for measurement of the TGC's, the W^- boson production angle. The $\cos\theta^*$ and ϕ^* in the leptonic system are also measured clearly. For hadronic jets, the flavour and charge of the original quark is not measured. Thus, there arises a two-fold ambiguity in the decay angles of hadronically decaying W bosons, $(\cos\theta^*, \phi^*) \leftrightarrow (-\cos\theta^*, \pi + \phi^*)$. If both W boson decay hadronically, the polar angle of the W^- boson also has a two-fold ambiguity, $\cos\Theta_W \leftrightarrow -\cos\Theta_W$. This ambiguity is resolved by combining the jet charges of each pair of jets to determine the charge of each W. The difference in the two W charges is then used to determine the sign of $\cos\Theta_W$. For example, L3 determines the charge of each jet based on a jet-charge technique[27], to assign positive and negative charge to the reconstructed W bosons. The sign assignment is found to be correct 69% of the time at 183 GeV when the jets are correctly paired. The distributions of these phase-space angles at $192 - 202$ GeV from L3 are shown in Figure 8.

5.2 Extraction of TGC's

Several methods to extract anomalous couplings have been investigated in order to evaluate their sensitivity to the TGC's. As the result, all four experiments employed methods utilising so-called 'Optimal Observables' (OO) which project the relevant kinematical information sensitive to a certain TGC onto a one dimensional distribution[28]. If the differential cross section $d\sigma/d\Omega$ is expanded as a function of a TGC α:

$$\frac{d\sigma}{d\Omega}(\alpha) = C_0(\Omega) + \alpha C_1(\Omega) + \alpha^2 C_2(\Omega), \tag{9}$$
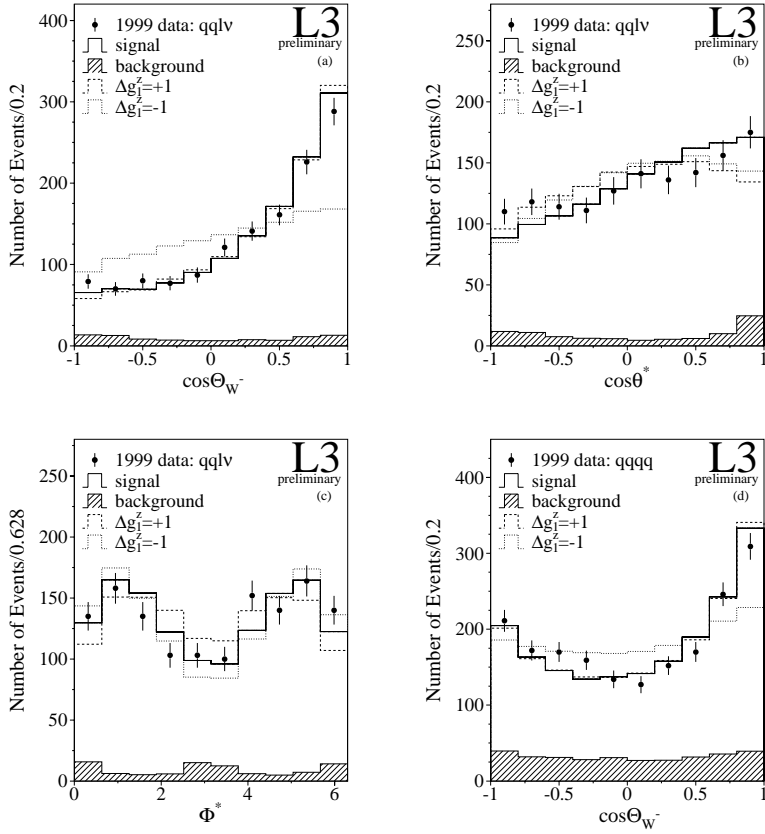
Figure 8: Distribution of reconstructed phase-space angles in selected data events at $192 - 202$ GeV from L3. (a) The polar angle of the W^- boson, $\cos\Theta_W$, for selected $q\overline{q}\,l\overline{\nu}_l$ events. (b) The polar decay angle of the leptonically decaying W boson, $\cos\theta^*$, for selected $q\overline{q}\,l\overline{\nu}_l$ events. (c) The azimuthal decay angle of the leptonically decaying W boson, ϕ^*, for selected $q\overline{q}\,l\overline{\nu}_l$ events. The value of ϕ^* is shifted by π for W^- decays in order to have the same ϕ^* distribution for W^- and W^+ decays. (d) The polar angle of the W^- boson, $\cos\Theta_W$, for selected $q\overline{q}q\overline{q}$ events. Open histograms show the Monte Carlo signal predictions, dashed histograms the background. As an example of the effects of anomalous couplings, distributions of these phase space angles for $\Delta g_1^Z = \pm 1$, normalized to the SM prediction, are shown as well.
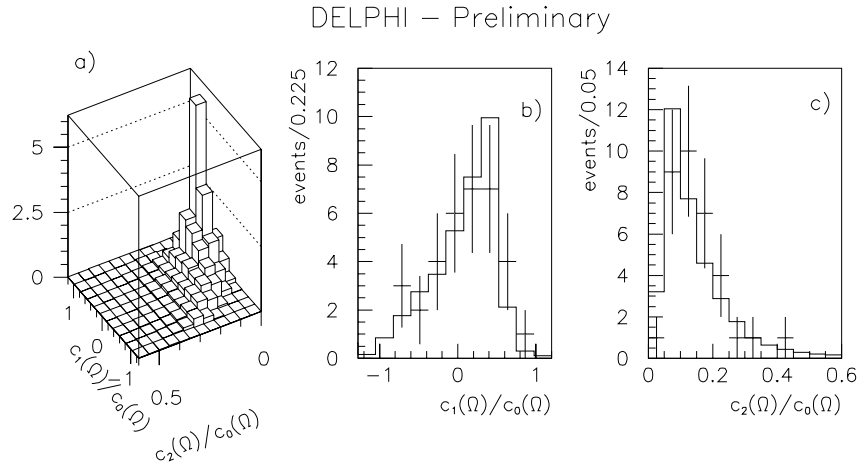
Figure 9: a) Distribution of $C_1(\Omega)/C_0(\Omega)$ versus $C_2(\Omega)/C_0(\Omega)$ for $\alpha_{W\phi}$ for 172 GeV data in the semileptonic channel. b) Projection onto the $C_1(\Omega)/C_0(\Omega)$ axis. c) Projection onto the $C_2(\Omega)/C_0(\Omega)$ axis. The points in b) and c) represent the data, and the histograms the expectation for the fitted value of $\alpha_{W\phi}$.
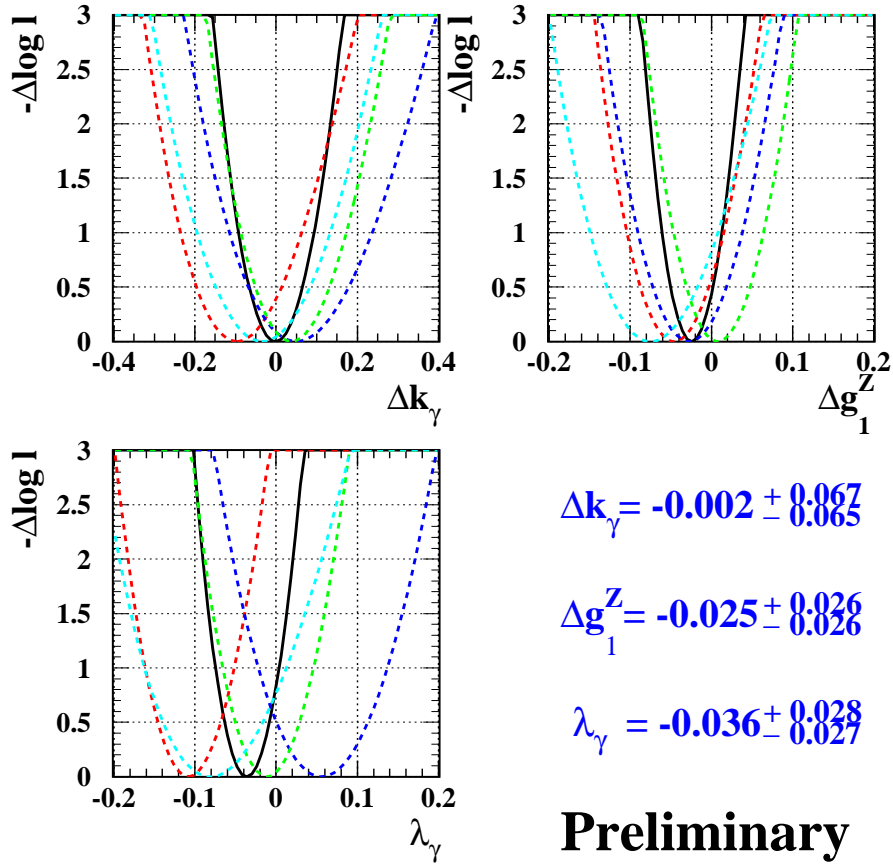
Figure 10: The LEP combined results of measurements on three TGC's, $\Delta\kappa_\gamma$, Δg_1^Z and λ_γ at LEP energies up to 202 GeV.

and it is differentiated by the TGC α as:

$$\frac{1}{C_0(\Omega)}\frac{d}{d\alpha}\frac{d\sigma}{d\Omega} = \frac{C_1(\Omega)}{C_0(\Omega)} + 2\alpha\frac{C_2(\Omega)}{C_0(\Omega)}, \tag{10}$$

the distributions of 2-variable space $(C_1/C_0, C_2/C_0)$ retains the whole information on a single parameter α. Thus a fit to $(C_1/C_0, C_2/C_0)$ allows the determination of a parameter α with maximum precision. For example, DELPHI analysed data at 172 GeV by performing a binned extended maximum likelihood fit to two-dimensional distribution of $(C_1/C_0, C_2/C_0)$ for each TGC parameter, where total cross section information is also included. Figure 9 shows the distribution of the data in the $(C_1/C_0, C_2/C_0)$ plane, together with its projections onto the two axes and the expected distributions for the fitted value of one TGC parameter, $\alpha_{W\phi}$.

Figure 10 shows the LEP combined results of the measured three TGC's, $\Delta\kappa_\gamma$, Δg_1^Z and λ_γ at LEP energies up to 202 GeV. As seen in the figure, the LEP combined results of three TGC's are obtained each by adding log $\mathcal{L}$ functions of four experiments. The log $\mathcal{L}$ functions from each experiment include statistical as well as all systematic uncertainties considered as uncorrelated between experiments. The systematic uncertainties are dominated by the sources

from theoretical WW cross section and fragmentation effect in hadronic W decays. The other sources of systematic errors are mainly from Bose-Einstein correlation and colour reconnection effects in fully hadronic channel. If the results from four experiments are combined, the statistical and systematic errors are comparable in size. These combined results of three TGC's are in good agreement with the Standard Model prediction.

6 Mass of the W boson

With the precise measurement of the mass of the W boson at LEP2 the situation for electroweak input parameters changes with respect to LEP1. The common practice at LEP1[29] is to use for M_W a value derived from the Fermi constant G_μ[17], which is accurately known from muon decay. The relation to obtain M_W follows from the Standard Model prediction for muon decay

$$G_\mu = \frac{\alpha\pi}{\sqrt{2}M_W{}^2(1 - M_W{}^2/M_Z{}^2)}\frac{1}{1 - \Delta r}, \tag{11}$$

where $\Delta r = 0$ at tree level and where Δr is m_t- and M_H-dependent when loop corrections are included. Thus, M_W in LEP1 calculations is m_t- and M_H-dependent through the above procedure. At LEP2, where one wants to measure M_W and, hence, wants to treat M_W as a fit parameter, the above relation now primarily acts as a test of the Standard Model. The above relation predicts for any chosen M_H and measured M_W a value for m_t that can be used as input for LEP2 loop calculations and can also be compared with the directly observed top-quark mass from the Tevatron[52,53].

As to the actual procedure to measure M_W from W-pair production, two methods are advocated. One procedure requires a measurement of the total W-pair cross section close to the threshold, where the size of σ_{tot} is most sensitive to the W mass. The other method looks at the decay products of the W boson and from the measured momenta of the decay products one tries to reconstruct the W mass.

6.1 W mass measurement by W-pair cross section

For an integrated $\mathcal{L}$ and an overall signal efficiency $\epsilon_{WW} = \sum \epsilon_i BR_i$ (where the sum extends over the various channels selected, with branching ratios BR_i and efficiencies ϵ_i), the error on the W^+W^- cross section due to signal statistics is given by

$$\Delta\sigma_{WW} = \frac{\sigma_{WW}}{\sqrt{N}} = \frac{\sqrt{\sigma_{WW}}}{\sqrt{\epsilon_{WW}\mathcal{L}}}, \tag{12}$$

where $N = \epsilon_{WW}\sigma_{WW}\mathcal{L}$ is the number of selected signal events. The corresponding error on the W mass is

$$\Delta M_W = \sqrt{\sigma_{WW}}\left|\frac{dM_W}{d\sigma_{WW}}\right|\frac{1}{\sqrt{\epsilon_{WW}\mathcal{L}}}. \tag{13}$$

The sensitivity factor $\sqrt{\epsilon_{WW}}\,|dM_W/d\sigma_{WW}|$ can be expressed as the function of $\sqrt{s} - 2M_W$ and this factor has a minimum value of approximately 0.91 GeV pb$^{-1/2}$ at

$$(\sqrt{s})^{opt} \simeq 2M_W + 0.5\text{GeV}. \tag{14}$$

This $(\sqrt{s})^{opt}$ of 161 GeV is taken as the starting CME of LEP2. In the actual procedure of measuring the W mass by W-pair cross section, equation 2 is employed again, where μ_i is given as a function of M_W and then the maximum likelihood value yields the measurement of the W mass. Figure 11 shows the results of W mass measurements by W-pair cross section from four experiments together with the combined result.
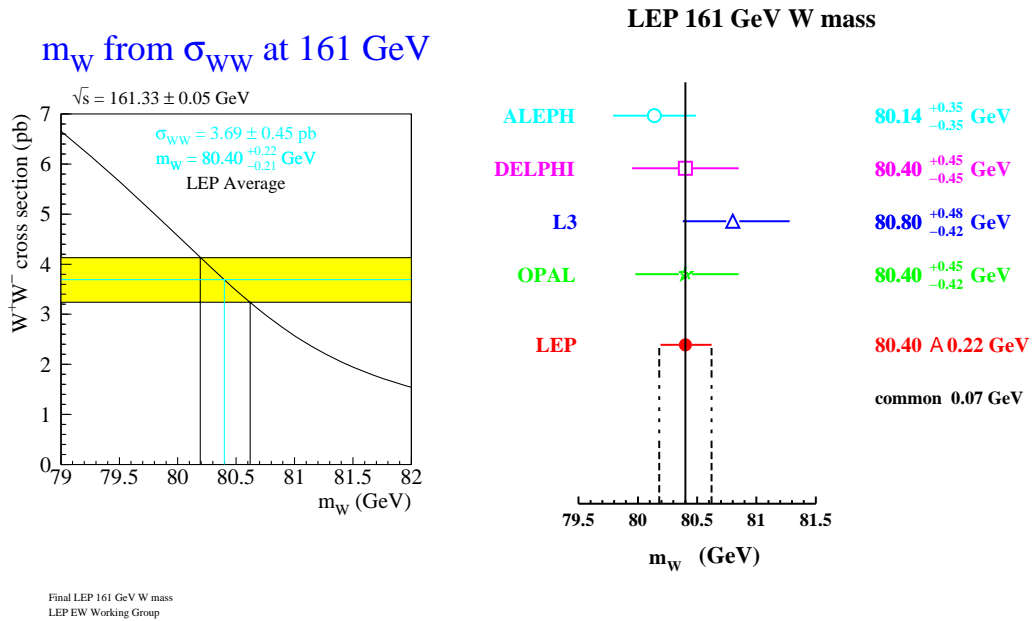
m_W from σ_WW at 161 GeV

√s = 161.33 ± 0.05 GeV

σ_WW = 3.69 ± 0.45 pb
m_W = 80.40 $^{+0.22}_{-0.21}$ GeV
LEP Average

W⁺W⁻ cross section (pb)

m_W (GeV)

Final LEP 161 GeV W mass
LEP EW Working Group

LEP 161 GeV W mass

ALEPH   80.14 $^{+0.35}_{-0.35}$ GeV

DELPHI   80.40 $^{+0.45}_{-0.45}$ GeV

L3   80.80 $^{+0.48}_{-0.42}$ GeV

OPAL   80.40 $^{+0.45}_{-0.42}$ GeV

LEP   80.40 A 0.22 GeV

common 0.07 GeV

m_W (GeV)

Figure 11: The results of M_W measurements by W-pair cross section at 161 GeV. Each error on the measured values is the quadratic sum of statistical and systematic uncertainties.

6.2   W mass measurement by direct reconstruction

At the CME's of 172 GeV, the sensitivity of the W-pair production cross section to the W mass is reduced, compared to the cross section at the threshold energy. Instead, at the all higher energies than 161 GeV, the measurement of the W mass can be made by direct reconstruction of the invariant mass of the fermion pairs from each W decay. A kinematic fit technique was employed in this method. Incorporating the constraints of energy and momentum conservation into a kinematic fit significantly improves the invariant mass resolution and is adopted by all experiments. A specific combination of additional constraints and techniques, for example, a constraint of equal mass of two W bosons, a technique of beam energy rescaling and so on, are chosen by some experiments. Events of the fully hadronic and semileptonic decay channels are used in the analyses. For each channel, several steps are needed to get the invariant mass distributions that are going to be used to extract the W mass.

In the fully hadronic channel, four jets in an event can be divided into two di-jets in three different ways. It is not obvious which of these partitions is correct and so this ambiguity leads to a combinatorial background. Four experiments employed different jet-pairing schemes to optimise the sensitivity to the W mass. For example, in OPAL analysis at 172 GeV, three kinematic fits were performed corresponding to the three combinations and placed an order with respect to the resulting fit probabilities. The combinations with the highest and second highest probabilities are used to extract the W mass information. At higher energies, OPAL adopted a likelihood method to determine the jet-pairing where kinematic variables of jets are used as inputs to the likelihood function.

In a $W^+W^-{\to}q\overline{q}\,l\overline{\nu}_l$ event ($l =$e or μ), a kinematic fit is performed including two jets and one lepton, imposing energy and momentum constraints. For $W^+W^-{\to}q\overline{q}\tau\overline{\nu}_\tau$ events, ALEPH employed kinematic fits, L3 and OPAL utilised a technique of beam energy rescaling. Figure 12 shows the distributions of the reconstructed invariant mass from DELPHI at 183 GeV for
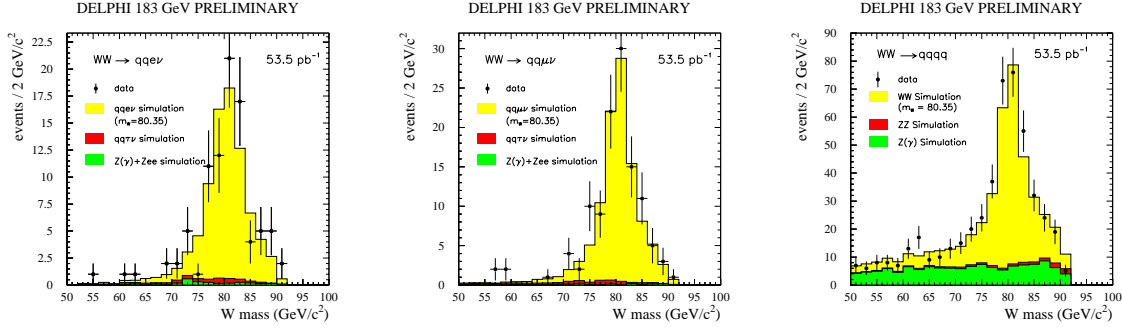
Figure 12: Reconstructed invariant mass distributions for $q\overline{q}e\overline{\nu}_e$ (left), $q\overline{q}\mu\overline{\nu}_\mu$ (center) and $q\overline{q}q\overline{q}$ (right) channels.

$q\overline{q}e\overline{\nu}_e$ (left), $q\overline{q}\mu\overline{\nu}_\mu$ (center) and $q\overline{q}q\overline{q}$ (right) channels, where a larger amount of background in fully hadronic channel than the semileptonic channel is due to the above mentioned jet-pairing combinatorial background.

The invariant mass distributions obtained from the event sample following the above procedures have a shape similar to the Breit-Wigner function, but sizably distorted due to several effects such as phase space restrictions, detector resolution, initial state radiation, background contamination, selection algorithms, etc... Then a simple Breit-Wigner fit without corrections would not give the right answer to the W mass measurements. The most straightforward method to overcome this fact is using a simple Breit-Wigner fit, correcting the result and its actual uncertainty with proper calibration curves obtained from the study of the distortion using sets of Monte Carlo samples at different M_W's.

Nevertheless, to make a more optimal use of the information in the data, one would prefer to fit directly to the data the invariant mass distribution predicted by the Monte Carlo, which has our best knowledge of all the fore-mentioned distortions already folded in. Then a possible way of extracting the value of M_W from the data sample would be to generate a large number of Monte Carlo events for various input values of M_W^{MC} and find the best matching Monte Carlo sample to the data sample, where the M_W^{MC} of that Monte Carlo sample yields the measurement of M_W.

However, given the time required for full simulation of each event, generating such many Monte Carlo samples with different M_W's, which would correspond to a resolution for M_W measurement, is unfeasible in practice. To overcome this difficulty, an alternative approach is to generate a large amount of Monte Carlo events at just some specific values of M_W and re-weight them with the matrix element ratio

$$w_i(M_W, \Gamma_W) = \frac{\left|\mathcal{M}(M_W, \Gamma_W, p_i^1, p_i^2, p_i^3, p_i^4)\right|^2}{\left|\mathcal{M}(M_W^{MC}, \Gamma_W^{MC}, p_i^1, p_i^2, p_i^3, p_i^4)\right|^2} \tag{15}$$

where $\mathcal{M}(M_W, \Gamma_W, p_i^1, p_i^2, p_i^3, p_i^4)$ is the matrix element of the process

$$e^+e^- \rightarrow W^+W^- \rightarrow f_1\bar{f}_2 f_3\bar{f}_4 \tag{16}$$

where p_i^j denotes the 4-momentum of the outgoing fermion j for a particular event i. The matrix element $\mathcal{M}$ is evaluated for the CC03 diagrams. This re-weighting method enables one to obtain a Monte Carlo sample with an arbitrary input value of M_W from the generated Monte Carlo samples with some specific values of M_W. ALEPH, L3 and OPAL employed this "re-weighting method" to extract the W mass at 172 GeV.

On the other hand, DELPHI developed a different method, so-called "convolution method", at 172 GeV. In this method, the information on the W mass is extracted from the likelihood

of observing each individual event. For example, in the case of semileptonic candidates, the likelihood is expressed as:

$$\mathcal{L}(M_\mathrm{W}) = P\left(\int_0^{E_b} G(m|m_\mathrm{f})BW(m|M_\mathrm{W})PS(m)dm\right) + (1-P)p_b(m_\mathrm{f}), \qquad (17)$$

where P is the overall fraction of events expected from simulation to be signal (90% for the electron events and 98% for the muon events). $G(m|m_\mathrm{f})$ is a Gaussian resolution function:

$$G(m|m_\mathrm{f}) = \frac{1}{\sqrt{2\pi}\sigma_\mathrm{f}} \exp\left(-\frac{(m-m_\mathrm{f})^2}{2\sigma_\mathrm{f}^2}\right), \qquad (18)$$

where m_f is the value of the fitted invariant mass and σ_f is the error on m_f. $BW(m|M_\mathrm{W})PS(m)$ is the expected distribution of the average of two W masses:

$$BW(m|M_\mathrm{W})PS(m) \propto \frac{\Gamma_\mathrm{W}}{M_\mathrm{W}} \frac{m^2}{(m^2 - M_\mathrm{W}^2)^2 + m^4\Gamma_\mathrm{W}^2/M_\mathrm{W}^2} \sqrt{E_b^2 - m^2}, \qquad (19)$$

where the width of the W resonance is taken as $\Gamma_\mathrm{W} = 2.07$ GeV. The shape of the background distribution, $p_b(m_\mathrm{f})$, is taken numerically from simulation.

For fully hadronic events, the expression is more involved due to the jet-pairing, where DELPHI treated not only 4-jet candidates but also 5-jet ones where 10 combinations of jet-pairing are possible. In the case of 4-jet events, the relative probability which gives the correct jet-pairing probability is estimated for all jet combinations. For the 5-jet candidates, each of the ten relative probabilities is determined with gluon radiation being taken into account. In addition, the efficiencies of the jet reconstruction are estimated for 4-jet and 5-jet events. All of these estimates are included in the expression of the likelihood for observing a fully hadronic event. It is noticed that the likelihood mentioned above is determined for an event. The combined likelihood for observing all the events is expressed as the product of all the event likelihoods. The maximum of this combined likelihood then yields the measurement of the W mass.

In the later stage of LEP2, all experiments adopted both re-weighting and convolution methods in each experiment. Two methods are used in each experiment to cross-check the results. Eventually, many efforts were made to develop common techniques to both methods to improve the sensitivity to the W boson mass. One of these works is the 5-jet analysis in OPAL. This technique was introduced in OPAL to reduce the statistical uncertainty of the re-weighting method in the fully hadronic final state. In this channel, hadronic jets in the detector were forced into a four jet topology to estimate the energy and momentum of the four quarks produced in the W decays. However, about 10% of fully hadronic events have at least one hard gluon emitted from one of primary quarks and tend to have a 5-jet-like event shape. This reduces the mass resolution and hence M_W sensitivity when the emitted gluon is (incorrectly) associated with a quark other than its parent. To avoid this difficulty, appropriate criteria were introduced to distinguish 5-jet events from 4-jet events, and the 5-jet-like events were forced into five jets naturally. These two samples were also treated differently in the subsequent fitting procedure. Figure 13 shows the reconstructed W mass distributions for $\mathrm{W^+W^-}\rightarrow\mathrm{q\bar{q}q\bar{q}}$ events divided into four and five jet samples at 189 GeV. The two left plots are for 4-jet sample and the two right plots for 5-jet sample. The upper plots show the distributions before the jet-pairing likelihood (JPLH) cut. The lower plots show the mass distributions which are used to determine the central value of W mass after the cut on JPLH. After introducing this 5-jet analysis, OPAL improved the W mass measurement sensitivity by 5%. DELPHI and OPAL achieved the best sensitivity to the W mass in fully hadronic channel among four experiments due to the efforts for the 5-jet analysis.
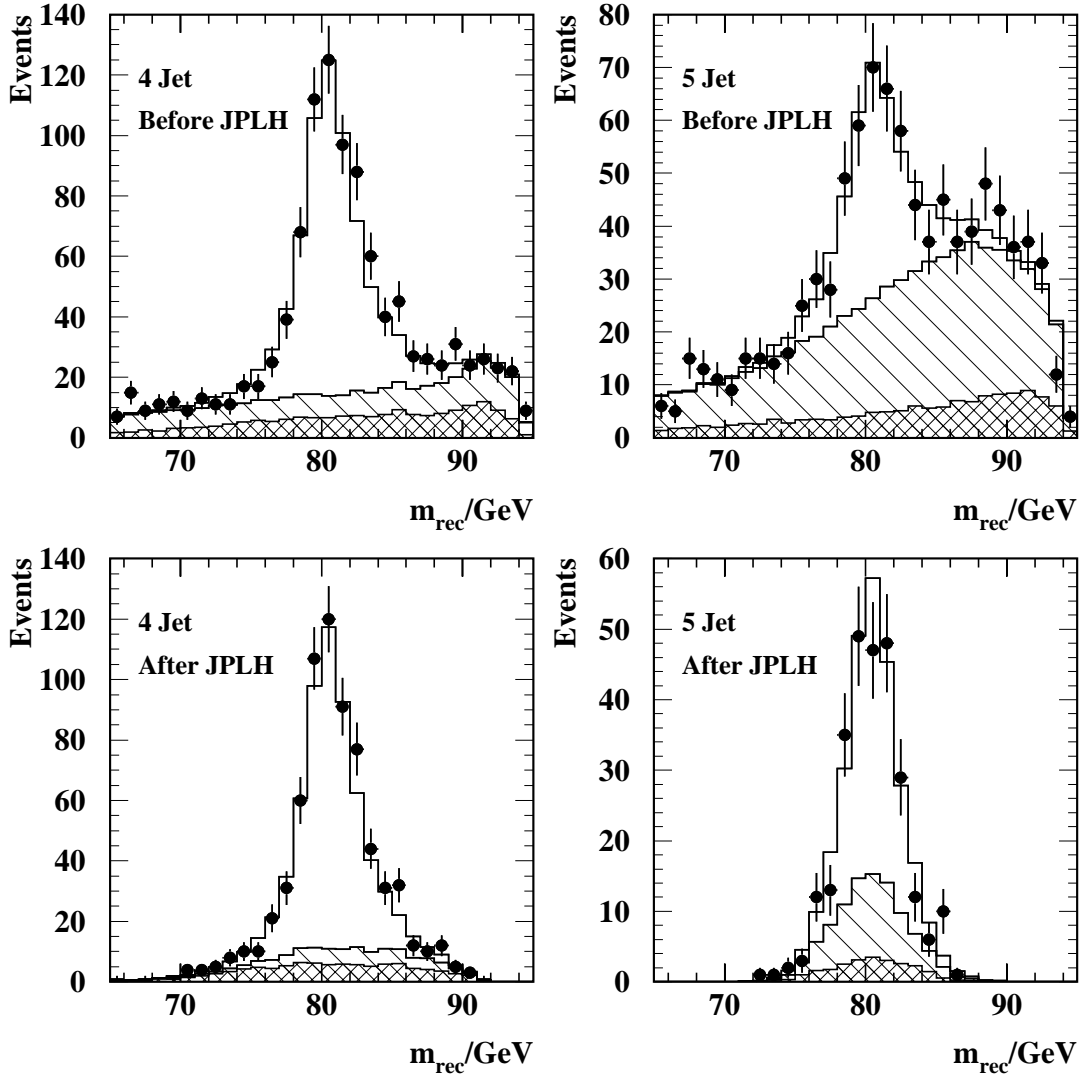
Figure 13: The reconstructed W mass distributions for $W^+W^- \rightarrow q\overline{q}q\overline{q}$ events divided into four and five jet samples. The upper plots show the distributions before the jet-pairing likelihood (JPLH) cut. The lower plots show the mass distributions which are used to determine the central value of W mass after the cut on JPLH. The points correspond to the OPAL data and the histograms to Monte Carlo predictions. The distribution from the non-WW background is shown as the cross-hatched histogram and the combinatorial background in indicated by the singly-hatched histogram.

Summer 2001 - LEP Preliminary

ALEPH [1996-2000]   80.456±0.060   ALEPH [1996-2000]   80.507±0.070

DELPHI [1996-2000]   80.414 ±0.089   DELPHI [1996-2000]   80.384±0.084

L3 [1996-2000]   80.314±0.087   L3 [1996-2000]   80.478±0.093

OPAL [1996-1999]   80.516±0.073   OPAL [1996-1999]   80.408±0.120

LEP   80.448±0.043   LEP   80.457±0.062

                     correl. with 4q = 0.28   correl. with non-4q = 0.28

LEP working group   LEP working group

80.0   81.0   80.0   81.0

M_W[GeV] (non-4q) M_W[GeV] (4q)

Figure 14: The results of W mass measurements by direct reconstruction for semileptonic (left) and fully hadronic (right) channels. Each error on the measured values is the quadratic sum of statistical and systematic uncertainties.

In semileptonic channel, ALEPH tried to utilise all pieces of information from the outputs of kinematic fits with different constraints. If a kinematic fit is performed with energy/momentum and the same W mass constraints, one obtains only one mass value and this can be a very sensitive mass estimator. However, a kinematic fit is performed with only energy/momentum constraints, one obtains two W masses, and these two variables includes some additional pieces of information on the W mass. Thus 3-dimensional fit with these three variables has a higher sensitivity to extract the W mass. ALEPH tried all combinations of output variables from kinematic fits, including W mass estimators and also their errors, for the extraction of W mass and finaly achieved the best sensitivity to the W mass in semileptonic channel.

Figure 14 shows the results of W mass measurement by direct reconstruction from four experiments for semileptonic (left) and fully hadronic (right) channels, as well as the LEP combination.

6.3 Systematic errors of W mass measurement

Table 7 shows the summary of error decomposition for the LEP combined M_W results. As seen in the table, the total systematic error is larger than the statistical error. Therefore, in the current stage of LEP W mass measurements, it is very important to reduce the systematic errors and rigorous efforts have been made to study those sources of systematic errors. Among those studies, three are described here in details, i.e. about the LEP beam energy, colour reconnection and Bose-Einstein correlation effects.

In the W mass measurements by direct reconstruction, the impact of LEP beam energy precision is quite direct. A kinematic fit with energy/momentum constraints improves the resolution of W mass measurement significantly, and the kinematic fit needs a precision measurement of LEP beam energy as input. The relation between the uncertainties of LEP beam energy and measured W mass is expressed as $\Delta M_w/M_w \sim \Delta E_{beam}/E_{beam}$. Currently, the error on LEP beam energy is about 20 MeV, and this error propagates to the uncertainty on the W mass to be 17 MeV. Thus if the precision on LEP beam energy is improved, the precision on W mass measurement can be achieved at this rate directly.

The present LEP2 beam energy calibration is performed in two steps. In the first step, the

Table 7: Summary of error decomposition for the LEP combined M_{W} results.

Source	Systematic Error on M_{W} (MeV)		
	$q\bar{q}\,l\bar{\nu}_l$	$q\bar{q}q\bar{q}$	Combined
ISR/FSR	8	9	8
Hadronization	19	17	17
Detector	12	8	10
LEP energy	17	17	17
Colour Reconnection	–	40	11
Bose-Einstein Correlation	–	25	7
Other	4	4	3
Total systematic	29	54	30
Statistical	33	30	26
Total	44	62	40

resonant depolarization technique is used to measure the beam energy below 60 GeV [30]. In this technique, the degree of beam polarization can be measured by the angular distribution of Compton-scattered polarized laser light. Then by exciting the beam with a transverse oscillating magnetic field, the transverse polarization can be destroyed when the excitation frequency matches the spin precession frequency. Determining the resonant depolarization frequency ν_s allows a precision determination of the beam energy E_b through

$$E_b = \frac{\nu_s m_e c^2}{(g_e - 2)/2} \tag{20}$$

where m_e is the electron mass, c is the speed of light and $(g_e - 2)/2$ the magnetic-moment anomaly of the electron. The intrinsic resolution of the resonant depolarization technique is about 200 keV. However, this technique works only up to $E_{beam} \sim 60$ GeV because necessary transverse polarization can not be achieved beyond this energy.

In the second step, the total bending field along the LEP ring is monitored during ramping the beam energy and the energy calibration can be extrapolated to higher energy, because of the relation:

$$E_b \propto \oint B_\perp dl. \tag{21}$$

There are two tools to measure the total bending field of LEP. The first tool is employing 16 NMR probes to measure the local magnetic field of reference dipoles in the LEP ring as seen in figure 15. The second tool is utilizing a flux-loop. A flux-loop covering the cross section of the dipole field has been placed inside the LEP dipoles as seen in figure 15. The voltage induced in this loop while cycling the magnets provides a measurement of the field integral produced by the LEP dipoles. The energy calibration method using these two tools achieves the resolution of 20 MeV.

In addition to this present method, two other methods have been studied to achieve the beam energy resolution of 10 MeV with combining the present measurements. One method is utilizing the relation between the synchrotron tune Q_s and E_b. Since the energy loss per turn, U_0, increases with the fourth power of energy

$$U_0 = (C_\gamma/\rho)E_b, \tag{22}$$

where C_γ is a constant depending on the particle type and ρ is the average bending radius, observables sensitive to the energy loss per turn can be used to determine the beam energy,
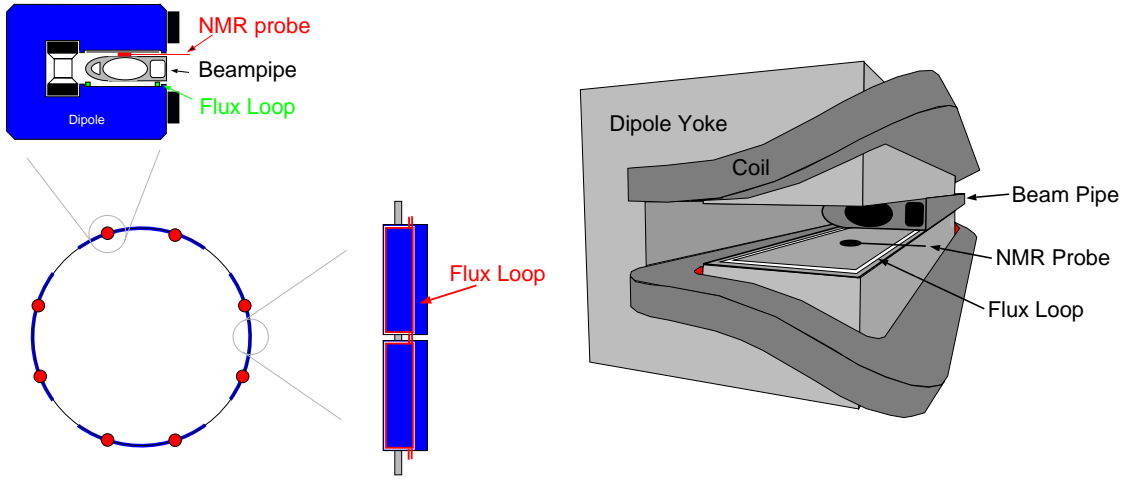
Figure 15: The layout of NMR probes and flux loop in LEP dipoles.

provided they can be measured and understood with sufficient precision. The synchrotron tune of the beam, Q_s, is such an observable. It has a dependence on the total effective accelerating voltage, V_{RF} and the energy loss as follows

$$Q_s^2 = (\frac{\alpha_c h}{2\pi E_b})\sqrt{e^2 V_{RF}^2 + b V_{RF}^4 - (U_0 + K)^2}, \qquad (23)$$

with α_c the optics dependent momentum compaction factor, and h the harmonic number (ratio between RF frequency and revolution frequency). bV_{RF}^4 accounts for the inhomogeneous distribution of the accelerating voltage around the ring. K represents energy loss from sources other than synchrotron radiation in the dipole magnets.

Measurements of Q_s as function of V_{RF} are used to extract the beam energy with a fit to this expression. The actual measurement of Q_s is based on a harmonic analysis of the measured phase difference between the bunch and RF signals. The uncertainty on the beam energy is about $20-25$ MeV and essentially energy independent. This includes statistical and systematic components. The systematic contributions to the error arise mainly from modelling of the total additional energy loss K. E_b has been measured using this method at the high energy points of 80 GeV (twice in 1999) and 90 GeV (once in 1998). The agreement between the measured values and the prediction of the NMR model is within errors of measurement. Additional three measurements were done in 2000 and the analysis is ongoing. These measurements are not yet included in the official values of LEP beam energy calibration which are used in the W mass analyses. These measurements will be combined with the present measurements of E_b in the near future.

The second additional method to measure E_b is by a spectrometer in the LEP ring. Figure 16 shows the principle of the LEP energy spectrometer. A dipole magnet is placed in the LEP ring, and the beam would be bended by the magnet field. The deflection angle is measured by six beam position monitors (BPMs) on either side of the dipole. Then the local beam energy can be measured in the ratio of the dipole bending field and the deflection angle as $E_b = (\frac{1}{\Delta\theta})\int B \, dl$.

This project was initiated in 1997 to install an in-line energy spectrometer into the LEP ring. An existing concrete LEP dipole was replaced with a precisely mapped steel dipole, and triplets of high precision beam position monitor (BPM) pickups were installed on either side of the dipole. Figure 17 shows the layout of the LEP energy spectrometer. With a triplet lever arm of roughly 10 meters, the BPMs must have a precision of 1 μm in the bending plane, and be stable against mechanical and electronic drifts at this level. Four NMR probes are mounted locally in the spectrometer dipole to measure a reference field value B_{ref}, and the total integral bending
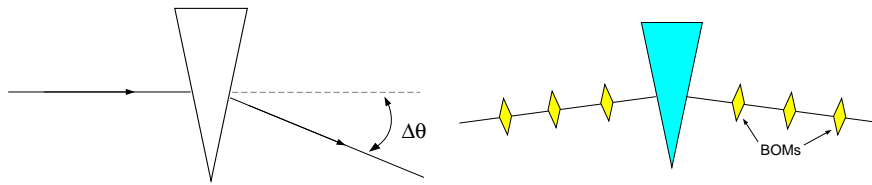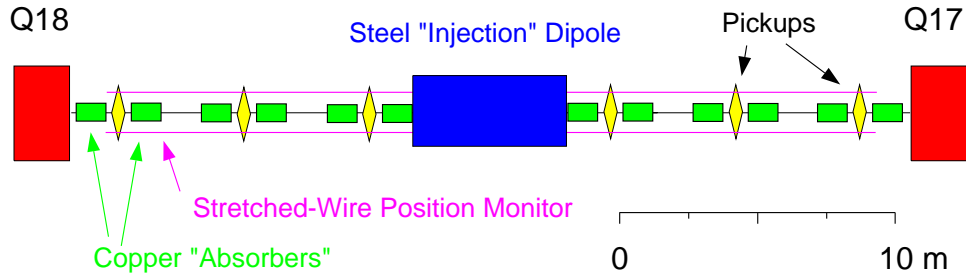
Figure 16: The principle of LEP spectrometer.

Figure 17: The layout of LEP spectrometer.

field has been determined as a function of B_{ref}. In the end field region temperature-stabilized Hall probes are also mounted to complete the field mapping. Using these NMR probes with an intrinsic relative precision of 10^{-6} and Hall probes with an intrinsic relative precision of 10^{-4}, a relative precision per map of 10^{-5} is achieved.

While a single arm prototype was installed in LEP for the 1998 run to test the mechanical design, the final spectrometer assembly was only completed towards the end of 1999 LEP run. Three fills have been used to perform a direct beam energy measurement using the spectrometer at physics energy in 1999 run. No bias was observed, and the scatter of the data seen at high energy is quite consistent with the expected uncertainty of 15 GeV. Analysis of data taken in 2000 run is ongoing. These measurements should be combined with the present E_b measurements to achieve the final goal of E_b resolution, i.e. 10 MeV, in the near future.

The Bose-Einstein effect is a positive correlation in narrow momentum space among identical bosons, i.e. pions of the same charge, produced in the hadronization process. This effect leads to an enhancement of the two-particle differential cross section for pair of identical pions close in phase space. The correlations were studied in the hadronic decays of the Z^0 at LEP1 [31,32], where a strong effect was observed. It has also been conjectured that the measurement of the W mass at LEP2 using fully hadronic 4-jet events is likely to be affected by Bose-Einstein correlations between pions from different W's [34].

For example, ALEPH analysis on Bose-Einstein correlation effects at 189 GeV is described here. The principle of the analysis is as follows: Bose-Einstein correlations are first analysed from a high statistics Z decay sample. The Bose-Einstein correlations for udsc quarks present in W decays are extracted from the natural mixture of udscb flavours in Z decays by means of b tagging. The distribution of Bose-Einstein correlations in these udsc flavours is well reproduced by a tuned version of a model of Lönnbald and Sjöstrand [35] implemented in JETSET. This Monte Carlo prediction is compared with the measurement of the Bose-Einstein correlations in $W^+W^- \rightarrow q\bar{q} \, l\overline{\nu}_l$ events and also in $W^+W^- \rightarrow q\bar{q}q\bar{q}$ under assumption that the two W's decay independently. Finally a variation of model (using a JETSET routine with model BE$_3$) [35] allowing Bose-Einstein correlations among different W's is tested by comparison with the $W^+W^- \rightarrow q\bar{q}q\bar{q}$ distribution.

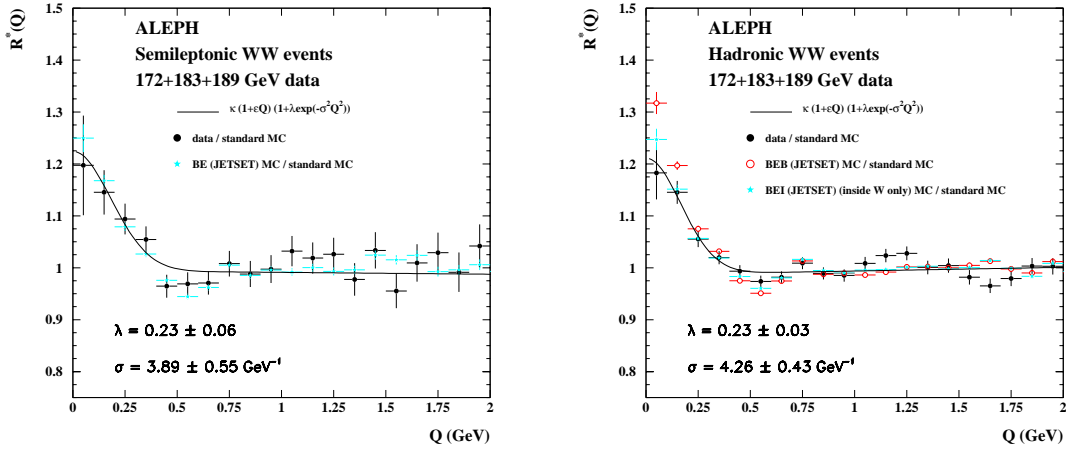In order to detect an enhancement of the two-particle cross section for pairs of identical

Figure 18: $R^*(Q)$ distributions for data and Monte Carlo with Bose-Einstein correlations for q$\overline{q}$ part of semileptonic WW events (left) and fully hadronic WW events (right). Only statistical errors are shown.

pions, a sample identical in all aspects with the like-charged pion pair sample, except for Bose-Einstein correlations, is needed as reference. The unlike-charged pion pairs are taken as the reference sample. The ratio of the number of like-charged pairs $(N^{++,--})$ to the number of unlike-charged pairs (N^{+-}) is measured as a function of $Q = \sqrt{(P_1 - P_2)^2 - (E_1 - E_2)^2}$, where $P_1 - P_2$ and $E_1 - E_2$ are the differences in 3-momentum and energy of the two particles. Then the correlation function $R(Q)$ is defined as

$$R(Q) = \frac{N^{++,--}(Q)}{N^{+-}(Q)}. \tag{24}$$

Since the unlike-charged pion pairs are not free from other sources of correlations, the correlation function $R(Q)$ is corrected by dividing by the same $R(Q)$ obtained from the Monte Carlo without Bose-Einstein correlations. In this way corrections for resonance decays and for acceptance effects are taken into account. This new ratio is called $R^*(Q)$ in the following, with:

$$R^*(Q) = \frac{R(Q)^{data}}{R(Q)^{MC}_{noBE}}. \tag{25}$$

This distribution is fitted with the formula from [31]:

$$R^*(Q) = \kappa(1 + \epsilon Q)(1 + \lambda \exp(-\sigma^2 Q^2)) \tag{26}$$

where κ is the normalization factor and the term $1 + \epsilon Q$ takes into account some long-range correlations, due to charge conservation or energy-momentum conservation. The $1 + \lambda \exp(-\sigma^2 Q^2)$ factor describes the Bose-Einstein effect. The parameter σ gives the source radius and λ the strength of the correlation between pions.

Figure 18 shows the $R^*(Q)$ distributions for data and Monte Carlo with Bose-Einstein correlations for q$\overline{q}$ part of semileptonic WW events (left) and fully hadronic WW events (right). For fully hadronic events, two Monte Carlo samples are used. One sample is without Bose-Einstein correlations between decay products of different W's ("BEI", Bose-Einstein inside), and other is with ("BEB", Bose-Einstein both). This figure shows that the Monte Carlo is very good agreement with the semileptonic data, and concerning fully hadronic W-pair decays, there is a better agreement between data and the Monte Carlo when Bose-Einstein correlations between decay products of different W's are excluded. In both fits, their inclusion is disfavoured at the 2.7σ level.
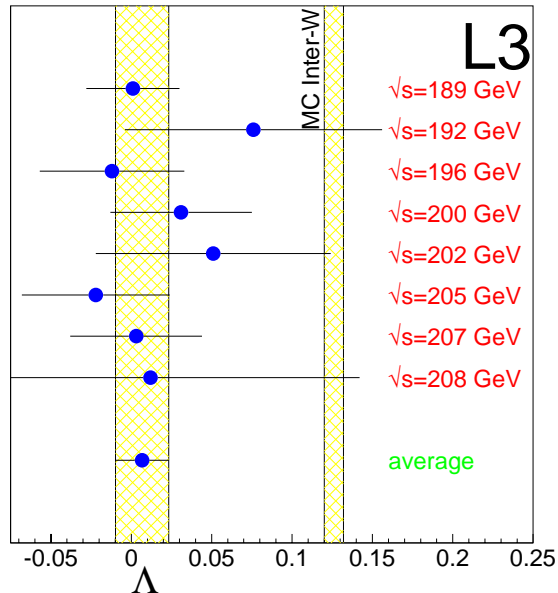
Figure 19: Value of the Λ parameter found at the different center-of-mass energies. The error is statistical only. Also shown is the Monte Carlo prediction of KORALW with Bose-Einstein correlation between different W's.

Other three experiments performed analyses on Bose-Einstein correlation effects with reference samples of deferent definitions. However, all four experiments found no evidence of Bose-Einstein correlations between different W's. Figure 19 shows measurements of Λ from L3 ($= \lambda$ in ALEPH convention), which represents the strength of Bose-Einstein correlation, with data at 189 – 208 GeV. Also shown in the figure is the Monte Carlo prediction of KORALW with Bose-Einstein correlation between different W's. As seen in the figure, the data favours no Bose-Einstein correlations between different W's. Four experiments assign systematic errors of 20 – 70 MeV in fully hadronic channel for Bose-Einstein correlation effects in the W mass measurements. These values are obtained from comparisons of measured W masses among Monte Carlo samples with and without Bose-Einstein correlation effects. 25 MeV is assigned in fully hadronic channel for the LEP average of the systematic error from the Bose-Einstein correlation effect as seen in table 7.

In W pair-productions, the average space time distance of the decay vertices of the two W bosons in the given energy range is about 0.1 fm, whereas the typical hadronic fragmentation scale is about 1 fm. Consequently, the two decay systems overlap in space time and may no longer fragment independently [36]. As a result the colour flow pattern of these events are modified and colour rearrangement between two colour singlets are expected from simple QCD principle. During the parton shower, Colour Reconnection (CR) effects are suppressed in the hard perturbative phase. However, during the fragmentation phase, CR between the two systems may occur as final state interactions [37].

Followings describes the analysis by L3 using the new method [38] based on the study of the energy- and particle-flow distributions in 4-jet events to search for the effects of particle depletion and enhancement in a model independent way. In this analysis, the energy and particle flows in the inter-jet regions are studied. First, the naming convention of jets and W bosons in each event is defined. The selected fully hadronic events are forced into four jets in an event and each

jet is assigned to a W boson by a jet pairing method. The most energetic jet is named as Jet-1, the W boson associated with the Jet-1 is called W-1, and the other jet from W-1 is called Jet-2 in each event. The rest of W boson is called W-2 and the two jets from W-2 are called Jet-3 and Jet-4, where jet-3 has higher energy than jet-4.

In the absence of colour reconnection, two strings are stretched between jet-1 and jet-2, and between jet-3 and jet-4. In case of colour reconnection a string is stretched between, for example, jet-1 and jet-3. The modification of such string topology may result in depletion and/or enhancement of soft particles in the inter-jet region of jet-1 and jet-3, and/or other combinations of two jets. To measure these effects, four planes and four inter-jet angles are defined in each event as follows. Plane-i is defined by two jets, jet-i and jet-$(i+1)$, where i runs from 1 to 4 and in case of plane-4, jet-5 = jet-1. The four angles are defined by two jets, jet-i and jet-$(i+1)$ on plane-i. Using these definitions, all particles from the fragmentation process can be projected onto these four planes and the rescaled angle is assigned to each particle-j as:

$$\phi_j^{resc} = \frac{\phi_j}{\phi_{i,i+1}} + (i-1). \tag{27}$$

where $\phi_{i,i+1}$ is the angle between jet-i and jet-$(i+1)$, which defines the plane-i, and ϕ_j is projected angle of particle-j onto plane-i. In this definition, jet-i has $\phi^{resc} = i - 1$, and particles between jet-1 and jet-2 have rescaled angles between 0 and 1, particles between jet-2 and jet-3 have rescaled angles between 1 and 2, and so on. Figure 20 (top) shows the particle-flow distributions obtained with PYTHIA Monte Carlo at 189 GeV for particles with a momentum greater than 100 MeV. The full line corresponds to no colour reconnection (No CR) while the dashed line corresponds to the prediction from the SKI 100 % model implemented in PYTHIA. The inter-jet regions between two jets from the same W boson are named A and B while the inter-jet regions between two jets from different W bosons are named C and D as shown in the figure (top). One can see that the SKI 100 % model gives some depletion of particle rates in the regions A and B, and some enhancement in regions C and D. The scaled angles are re-computed as:

$$\phi_j^{resc} = \frac{\phi_j}{\phi_{i,i+1}}, \tag{28}$$

and regions A and B, as well as regions C and D, can be averaged in order to reduce the statistical uncertainty. The averaged results are shown in the two bottom plots in Figure 20.

The ratio of the particle activity between the quarks from the same W (region A+B) and that from different W's (region C+D) is found to be a sensitive observable to the colour reconnection effect. This ratio computed from the particle-flow distributions as a function of the rescaled angle ϕ^{resc} is shown on the left side of Figure 21 for 189 – 207 GeV. The full line corresponds to the PYTHIA prediction without CR, the dashed line is the prediction from the SKI scenario, and the dotted line corresponds to the prediction of the SKI 100 % model. The dots are the L3 data. The same plot for the energy flow is shown on the right side of Figure 21, where the histogram for Figure 20 is filled with energies carried by particles and the ratio is computed in the same way.

For both plots in Figure 21, the differences between the models with and without reconnection schemes are larger in the middle of the inter-jet regions. Therefore, in order to quantify the colour reconnection effects, the integrated ratio R is computed in a restricted ϕ^{resc} interval ranging from 0.2 to 0.8. The corresponding variables for particle and energy flows are defined as follows:

$$R_N = \frac{\int_{0.2}^{0.8} \frac{1}{N_{evt}} \frac{dn}{d\phi}(region\ A+B)d\phi}{\int_{0.2}^{0.8} \frac{1}{N_{evt}} \frac{dn}{d\phi}(region\ C+D)d\phi} \qquad and \qquad R_E = \frac{\int_{0.2}^{0.8} \frac{1}{E_{evt}} \frac{dE}{d\phi}(region\ A+B)d\phi}{\int_{0.2}^{0.8} \frac{1}{E_{evt}} \frac{dE}{d\phi}(region\ C+D)d\phi}. \tag{29}$$
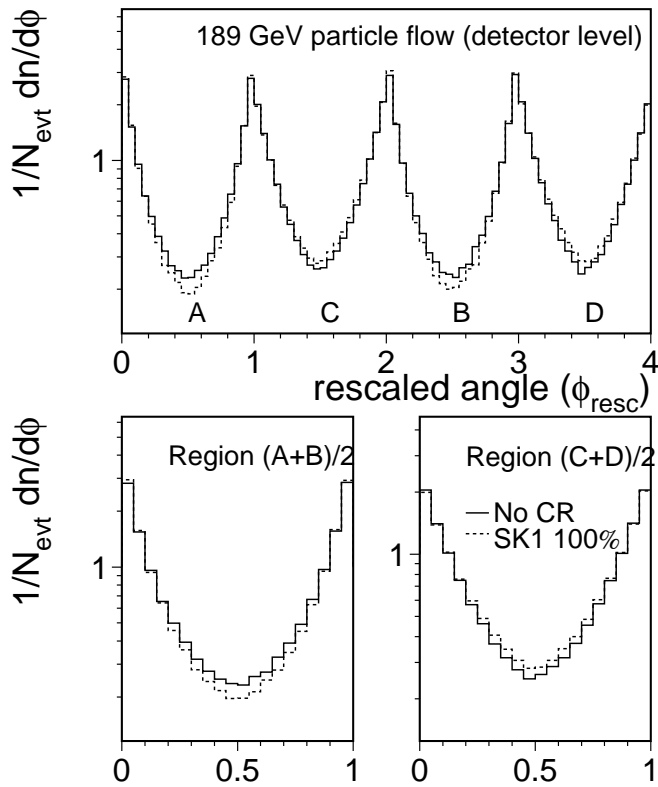
Figure 20: PYTHIA prediction at 189 GeV for particle-flow distribution without colour reconnection (No CR) and for the SKI 100 % model.
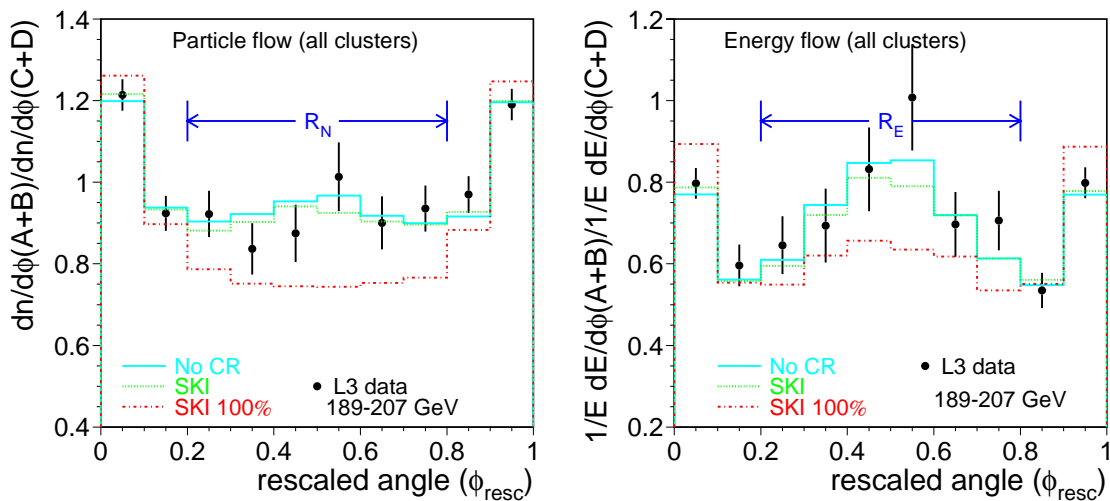

Figure 21: Ratio (R) of the flow distribution in region (A+B) divided by the flow distribution in region (C+D) for particle on the left and for energy on the right.
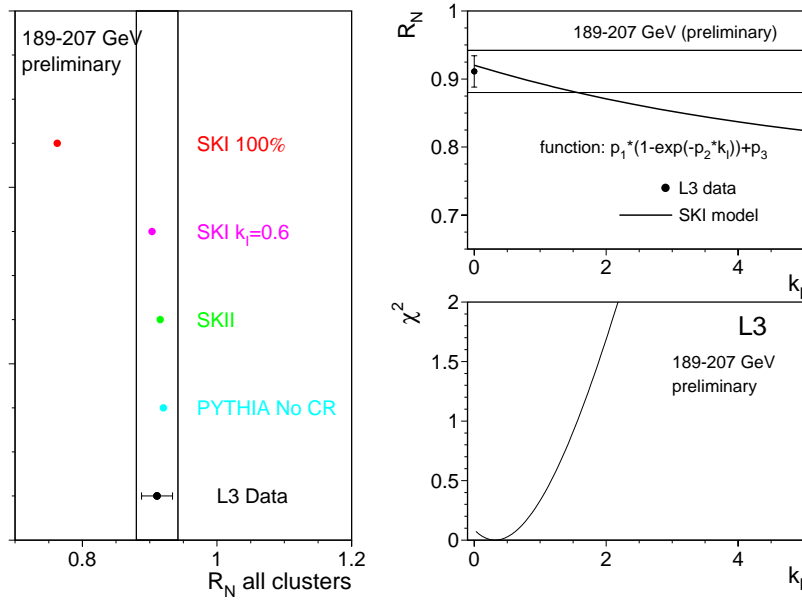
Figure 22: Left-hand side: the ratio R_N for several Monte Carlo models with and without colour reconnection. The black dot with the error bar shows the L3 data with the statistical error only while the band corresponds to the sum of the statistical and systematic errors in quadrature. Right-hand side (top): the ratio R_N fitted as a function of k_I for the SKI model. The black dot with the error bar shows the L3 data with the statistical error only while the band corresponds to the sum of the statistical and systematic errors in quadrature. Right-hand side (bottom): a χ^2 curve obtained by comparing the L3 data to the SKI predicted dependence.

The sensitivity of R_N to colour reconnection effects is larger than that of R_E and both ratios are strongly correlated. Thus the following results are based on only R_N. Figure 22 (left-hand side) shows a comparison of measured R_N's at $189 - 207$ GeV among the data, Monte Carlo samples with several colour reconnection models and also a sample without colour reconnection. The dot with error shows the L3 data value with the statistical error only while the band corresponds to the total error taken as the sum of the statistical and systematic components in quadrature. In order to see the dependence of R_N on the reconnection probability of the SKI model, three Monte Carlo are used: the one generated with 100 % reconnection probability, the standard sample with $k_I = 0.6$ and the No CR sample. As seen in the figure, the data are not showing strong colour reconnection effects when compared to these PYTHIA models.

In the SKI model the fraction of reconnected events is controlled by the k_I parameter and a parametrisation of the ratio dependence on k_I has been attempted with the three available Monte Carlo samples. Figure 22 (Right-hand side, top) shows the k_I dependence of R_N where the solid curve is obtained by fitting to the three SKI samples. The black dot is the L3 data measurement of R_N with the horizontal band showing the one σ boundary including the systematic error. A χ^2 between the data and Monte Carlo samples is evaluated as a function of k_I and the result is shown in Figure 22 (Right-hand side, bottom). This curve gives a minimum at $k_I = 0.32$, corresponding to about 18 % reconnection probability at 189 GeV, with a large uncertainty making the result also consistent with no CR effect. Then an upper limit $k_I < 1.55$ is obtained at 68 % C.L. using whole L3 data sample. This value should corresponds to a reconnection probability of about 50 % at 189 GeV. First checks of the effect on the W mass reconstruction yielded a mass shift of about +75 MeV at 189 GeV in L3.

This L3 result of the W mass shift seems discouraging, however, the following OPAL analysis might reduce this large shift of 75 MeV. OPAL has been studying several W mass analysis methods which are insensitive to the colour reconnection effects in terms of the W mass measurement. If colour reconnection occurs, the string stretched between two jets from different
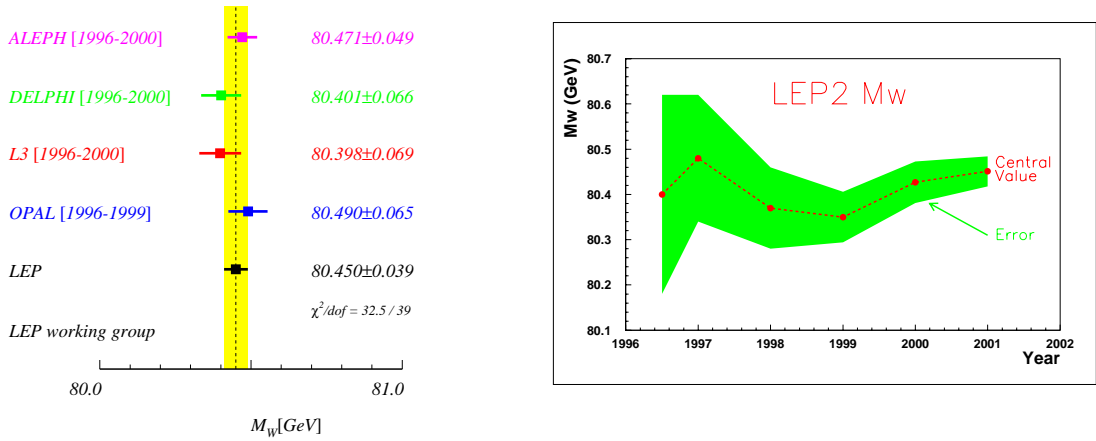
Figure 23: Left-hand side: the LEP combined result of W mass measurements by cross section measurement and direct reconstruction, where each error on the measured values is the quadratic sum of statistical and systematic uncertainties. Right-hand side: a history of LEP W mass measurements as a function of the year, where the band shown in the figure denotes the error of W mass measurements and the solid line indicates the central values of the measured W mass.

W's results in soft particles in the inter-jet region of the two jets. Thus if one applies a cut on particles with a momentum greater than 100 MeV, and perform W mass reconstruction based on particles after this cut, the measured value of W mass can be made rather insensitive to the colour reconnection effects. The OPAL default analysis gives about 100 MeV W mass shift when assuming 50 % colour reconnection probability. However, if the above CR insensitive W mass measurement is performed, the W mass shift can be reduced to about 30 MeV without losing much sensitivity to the W mass. If four experiments further study the k_I parameter of SKI model with particle- and energy-flow methods and combine the results with the W mass measurement methods which are insensitive to colour reconnection effects, it is probable that the systematic error from the CR effects might be reduced to less than 30 MeV for each experiment.

6.4   Results of W mass measurement

Figure 25 (Left-hand side) shows the LEP combined result of W mass measurements by cross section measurement and direct reconstruction, where each error on the measured values is the quadratic sum of statistical and systematic uncertainties. Figure 25 (Right-hand side) shows a history of LEP W mass measurements as a function of year, where the band in the figure denotes the errors of LEP W mass measurements and the solid line indicates the central values of the LEP W mass measurements.

6.5   Discussions

The W mass measurements at the threshold and higher energies together with other precise electroweak measurements performed at LEP[39] are used to check the validity of the Standard Model and, within its framework, to infer valuable information about its fundamental parameter, in particular the top-quark mass, m_t, and Higgs boson mass, M_H, through loop corrections. In this procedure, to obtain the best sensitivity also used are: the results from SLD[39,40] as well as measurements of M_W from UA2[41], CDF and DØ[42,43,44,45], measurements of the top-quark mass by CDF and DØ[52,53,54], measurements of the neutrino–nucleon neutral to charged current ratios
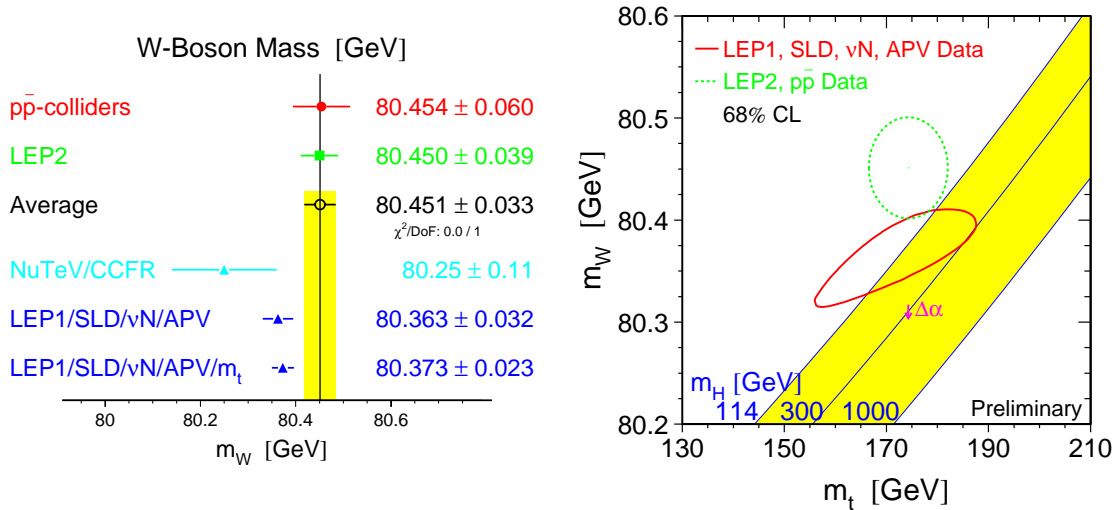
Figure 24: Left-hand side: the world averages of direct (Tevatron and LEP2) and indirect (LEP1+SLD+νN+APV) W mass measurements. Right-had side: the comparison of the indirect measurements of M_W and m_t (LEP1+SLD+νN+APV data) (solid contour) and the direct measurements (Tevatron and LEP2 data) (dashed contour). In both cases the 68% C.L. contours are plotted. Also shown is the Standard Model relationship for the masses as a function of the Higgs mass.

from CCFR[46] and NuTeV[47], and measurements of atomic parity violation (APV) in cesium[48,49] with the numerical result taken from [50,51]. Additional input parameters are the Fermi constant G_F, determined from the μ lifetime, $G_F = 1.16637(1) \times 10^{-5}$ GeV^{-2}[55], and the photon vacuum polarization of $\Delta\alpha_{had}^{(5)}(m_Z^2) = 0.02761 \pm 0.00036$[57].

To test the consistency of the Standard Model, a comparison of the world averages of direct and indirect W mass measurements is performed. Figure 24 (left-hand side) shows the world averages of direct (Tevatron and LEP2) and indirect (LEP1+SLD+νN+APV) W mass measurements. The direct measurement is slightly larger than the indirect measurements, although these are in agreement within the errors.

In addition, a fit to the indirect data leaving the top quark and W masses as free parameter is performed. The result can be compared with the direct measurements of the top and W masses performed at Tevatron and LEP2. The comparison can be plotted on the W- and top-mass plane in contour style. Figure 24 (right-hand side) shows the comparison of the indirect measurements of M_W and m_t (LEP1+SLD+νN+APV data) (solid contour) and the direct measurements (Tevatron and LEP2 data) (dashed contour). In both cases the 68% C.L. contours are plotted. Also shown is the Standard Model relationships to the top and W masses as a function of Higgs-mass values between 114 and 1000 GeV. As seen in the figure, the direct measurements prefer high M_W and low M_H.

Finally, the best constraints on M_H are obtained when all data, indirect and direct measurements, are used in the fit. The results of this fit are shown in Figure 25. In this figure, the observed value of $\Delta\chi^2 = \chi^2 - \chi^2_{min}$ as a function of M_H is plotted for the fit including all data. The dashed band represents the uncertainty due to uncalculated higher-order corrections. The 95 % C.L. upper limit on M_H (taking the band into account) is 196 GeV. The lower limit on M_H of approximately 114 GeV obtained from direct searches[56] is not used in the determination of this limit. Also shown is the result (dashed curve) obtained when using $\Delta\alpha_{had}^{(5)}(m_Z^2)$ of Reference [58]. That fit results in $\log(M_H/\text{GeV}) = 2.03 \pm 0.19$ corresponding to $M_H = 106^{+57}_{-38}$ GeV and an upper limit on M_H of approximately 222 GeV at 95 % confidence level.
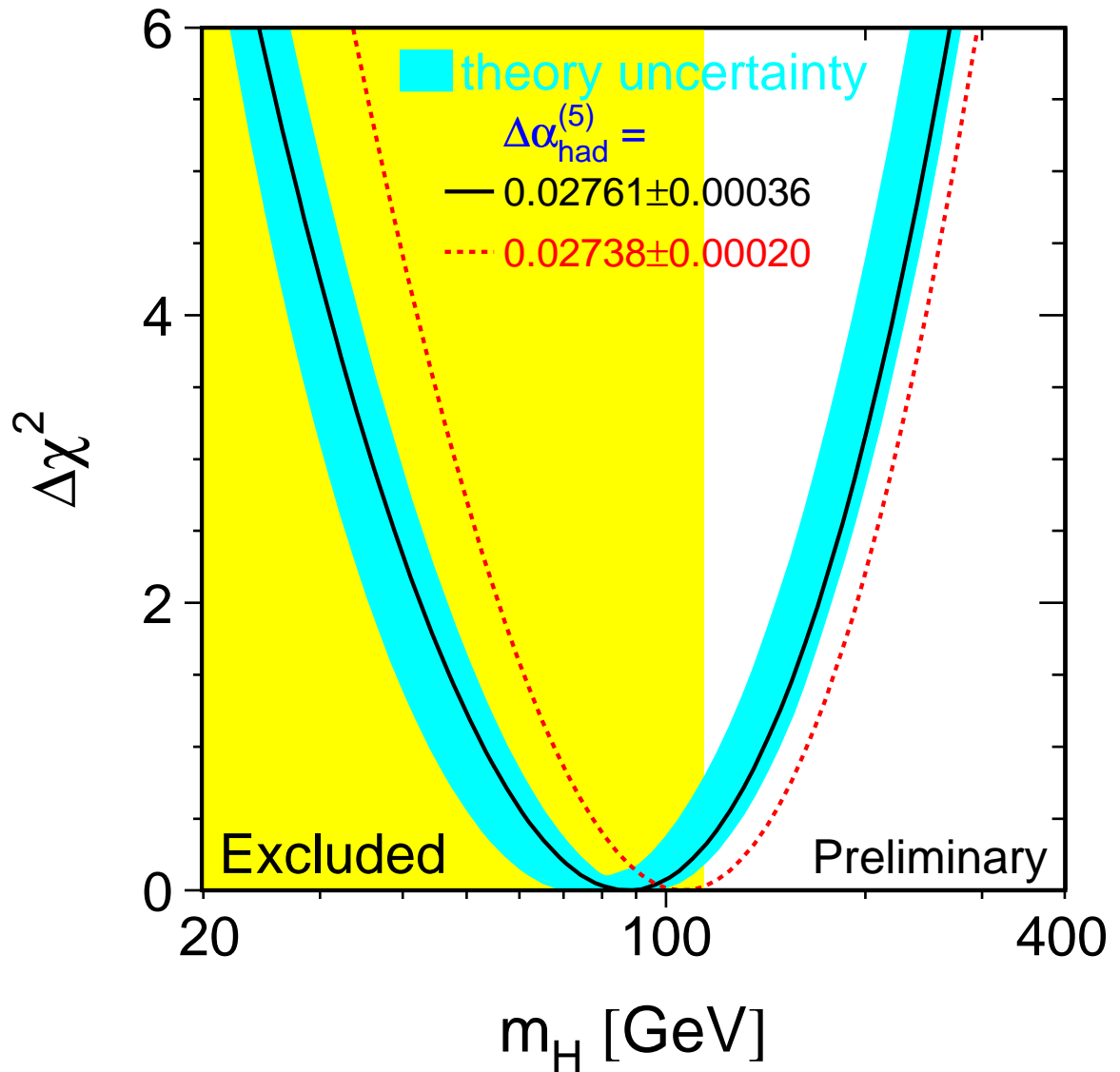
Figure 25: $\Delta\chi^2 = \chi^2 - \chi^2_{min}$ vs. m_H curve. The line is the result of the fit using all data; indirect and direct measurements. The band represents an estimate of the theoretical error due to missing higher-order corrections. The vertical band shows the 95 % C.L. exclusion limit on m_H from the direct search. The dashed curve is the result obtained using $\Delta\alpha^{(5)}_{had}\ (m_Z^2) = 0.02738 \pm 0.00020$.

7 Summary

LEP2 started at the energy just above the W-pair production threshold in 1996 and raised the energies to significantly above the threshold. At the energies of 161 – 209 GeV, it enabled the four experiments, ALEPH, DELPHI, L3 and OPAL to study the physics on W-pair production in clean environment of e^+e^- collisions. The data acquisition of LEP experiments was finished on 2nd November 2001. The main combined results of four experiments on WW physics are; good agreements between the measured W-pair cross sections and the predictions of YFSWW and RACOONWW, W-pair branching fraction: $Br(W \to hadron) = 67.92 \pm 0.27\%$ and $Br(W \to lepton) = 10.69 \pm 0.09\%$, improvement on CKM matrix element: $|V_{CS}| = 0.996 \pm 0.013$, three TGC's: $\Delta\kappa_\gamma = -0.002^{+0.067}_{-0.065}$, $\Delta g_1^Z = -0.025^{+0.026}_{-0.026}$, and $\lambda_\gamma = -0.036^{+0.028}_{-0.027}$ and mass of W: $M_W = 80.450 \pm 0.039$ GeV. All results are in agreement with the Standard Model expectations. The world average of the direct measurements of W mass is slightly larger than that of the indirect measurements, although two measurements are within measurement errors. Combining LEP results with electroweak measurements from other experiments, the 95 % C.L. upper limit of 196 GeV is obtained on Higgs mass M_H.

Acknowledgments

References

1. ALEPH Collaboration, Nucl. Instrum. Meth. **A294** (1990) 121; ALEPH Collaboration, Nucl. Instrum. Meth. **A360** (1995) 481.
2. DELPHI Collaboration, Nucl. Instrum. Meth. **A303** (1991) 233; DELPHI Collaboration, Nucl. Instrum. Meth. **A378** (1996) 57.
3. L3 Collaboration, Nucl. Instrum. Meth. **A289** (1990) 35; M. Chemarin *et al.*, Nucl. Instrum. Meth. **A349** (1994) 345; M. Acciarri *et al.*, Nucl. Instrum. Meth. **A351** (1994) 300; G. Basti *et al.*, Nucl. Instrum. Meth. **A374** (1996) 293; I. C. Brock *et al.*, Nucl. Instrum. Meth. **A381** (1996) 236; A. Adam *et al.*, Nucl. Instrum. Meth. **A383** (1996) 342.
4. OPAL Collaboration, Nucl. Instrum. Meth. **A305** (1991) 275; P. P. Allport *et al.*, Nucl. Instrum. Meth. **A324** (1993) 34; P. P. Allport *et al.*, Nucl. Instrum. Meth. **A346** (1994) 476.
5. T. Sjöstrand, Pythia 5.7 / Jetset 7.4, CERN-TH.7112/93 (1993).
6. S. Jadach, W. Placzek, M. Skrzypek, B. F. L. Ward, Phys. Rev. **D54** (1996) 5434; S. Jadach, W. Placzek, M. Skrzypek, B. F. L. Ward, Z. Wąs, Phys. Lett. **B417** (1998) 326; S. Jadach, W. Placzek, M. Skrzypek, B. F. L. Ward, Z. Wąs, Phys. Rev. **D61** (2000) 113010: CERN-TH-99-222, hep-ph/9907346; S. Jadach, W. Placzek, M. Skrzypek, B. F. L. Ward, Z. Wąs, CERN-TH/2000-337, hep-ph/0007012: submitted to Phys. Lett. **B**; S. Jadach, W. Placzek, M. Skrzypek, B. F. L. Ward, Z. Wąs, CERN-TH/2001-017, hep-ph/0103163: accepted by Comput. Phys. Commun.
   The YFSWW cross sections at 155 – 215 GeV have been kindly provided by the authors.
7. A. Denner, S. Dittmaier, M. Roth and D. Wackeroth, Nucl. Phys. **B560** (1999) 33; A. Denner, S. Dittmaier, M. Roth and D. Wackeroth, Nucl. Phys. **B587** (2000) 67; A. Denner,

S. Dittmaier, M. Roth and D. Wackeroth, Phys. lett. **B475** (2000) 127; A. Denner, S. Dittmaier, M. Roth and D. Wackeroth, hep-ph/0101257.
The RACOONWW cross sections at 155 – 215 GeV have been kindly provided by the authors.

8. M. W. Grünewald, G. Passario et al., Four fermion working group report of the LEP2 Monte Carlo Workshop 1999/2000, hep-ph/0005309.

9. See [8] and references therein for a discussion of complete $O(\alpha)$ radiative corrections to W-pair production in the LPA/DPA approximations.

10. The theoretical uncertainty $\Delta\sigma/\sigma$ on the W-pair production cross section calculated in the LPA/DPA above 170 GeV can be parametrized as $\Delta\sigma/\sigma = 0.4 \oplus 0.072 \cdot t_1 \cdot t_2$ where $t_1 = (200 - 2 \cdot M_w)/(\sqrt{s} - 2 \cdot M_w)$ and $t_2 = (1 - (3 \cdot M_w/300)^3)/(1 - (3 \cdot M_w/\sqrt{s})^3)$. In the threshold region, a 2 % uncertainty is assigned. Private communication from the authors of [6,7].

11. D. Bardin, J. Biebel, D. Lehner, A. Leike, A. Olchevski and T. Riemann, Comp. Phys. Comm. **104** (1997) 161. See also [8].

12. M. Skrzypek, S. Jadach, M. Martinez, W. Placzek, Z. Wąs, Phys. Lett. **B372** (1996) 289; S. Jadach, W. Placzek, M. Skrzypek, Z. Wąs, Comp. Phys. Comm. **94** (1996) 216; S. Jadach, W. Placzek, M. Skrzypek, B. F. L. Ward, Z. Wąs, hep-ph/0104049: submitted to Comp. Phys. Comm.;
The KORALW cross sections at 155 – 215 GeV have been kindly provided by the authors. They have actually been computed using YFSWW[6], switching off non-leading $O(\alpha)$ radiative corrections and the screening of the Coulomb correction, to reproduce the calculation from KORALW.

13. A. P. Chapovsky and V. A. Khoze, Eur. Phys. J. **C9** (1999) 449.

14. K. Melnikov and O. Yakovlev, Phys. Lett. **B324** (1994) 217. V. S. Fadin, V. A. Khoze and A. D. Martin, Phys. Rev. **D49** (1994) 2247.

15. W. Beenakker et al., "WW Cross-Section and Distributions", in "Physics at LEP2", eds. G. Altarelli et al., CERN 96–01.

16. Proceedings of CERN LEP2 Workshop, CERN 96-01, Vols. 1 and 2, eds. G. Altarelli, T. Sjöstrand and F. Zwirner, February 1996.

17. The Particle Data Group, E. D. Groom et al., Eur. Phys. J. **C15** (2000) 1.

18. P. Abreu et al., Phys. Lett. **B439** (1998) 209. R. Barate et al., Phys. Lett. **B465** (1999) 349.

19. CDF Collaboration, F. Abe et al., Phys. Rev. Lett. **75** (1995) 1017;
DØ Collaboration, S. Abachi et al., Phys. Rev. Lett. **75** (1995) 1023, S. Abachi et al., Phys. Rev. Lett. **77** (1996) 3303.

20. Physics at LEP2, Edited by G. Altarelli, T. Sjöstrand and F. Zwirner, Report on the LEP2 workshop 1995, CERN 96-01 (1996) Vol. 1 p525.

21. K. Hagiwara, R. Peccei, D. Zeppenfeld and K. Hikasa, Nucl. Phys. **B282** (1987) 253.

22. M. Bilenky, J. L. Kneur, F. M. Renard and D. Schildknecht, Nucl. Phys. **B409** (1993) 22.

23. M. Bilenky, J. L. Kneur, F. M. Renard and D. Schildknecht, Nucl. Phys. **B419** (1994) 240.

24. K. Gaemers and G. Gounaris, Z. Phys. **C1** (1979) 259.

25. A. De Rújula, M. B. Gavela, O. Pène and F. J. Vegas, Nucl. Phys. **B357** (1991) 311.

26. A. De Rújula, M. B. Gavela, P. Hernandez and E. Massó, Nucl. Phys. **B384** (1992) 3.

27. The L3 Collaboration, M. Acciarri et al., Phys. Lett. **B413** (1997) 176.

28. M. Diehl and O. Nacthmann, Zeit. Phys. **C62** (1994) 397.

29. D. Bardin, W. Hollik and G. Passarino (eds.), Reports of the working group on precision calculations for the Z resonance (CERN-95-03, Geneva, 1995).

30. The LEP Polarization Team, Z. Phys. **C66** (1995) 45 – 62; The LEP Energy Working

Group, Eur. Phys. J. **C6** (2) (1999) 187 – 223, CERN–EP/98–040, CERN–SL/98–012.

31. ALEPH Collaboration, D. Decamp *et al.*, Zeit. Phys. **C54** (1994) 75.
32. DELPHI Collaboration, P. Abreu *et al.*, Phys. Lett. **B286** (1992) 201.
33. The LEP Energy Working Group, Eur. Phys. J. **C11**, 573 – 585 (1999), CERN–EP/98–191, CERN–SL/98–073.
34. L. Lönnblad and T. Sjöstrand, Phys. Lett. **B351** (1995) 293.
35. L. Lönbald and T. Sjöstrand, Eur. Phys. J. **C2** (1998) 165.
36. G. Gustafson, U. Patterson and P. Zerwas, Phys. Lett. **B209** (1988) 90.
37. T. Sjöstrand and V. A. Khoze, Zeit. Phys. **C62** (1994) 281; V. A. Khoze and T. Sjöstrand, Eur. Phys. J. **C6** (1999) 271.
38. D. Duchesneau, *"New method based on energy- and particle-flow in $e^+e^- \rightarrow W^+W^- \rightarrow$ hadrons events for colour reconnection studies"*, preprint LAPP-EXP 2000-02. http://wwwlapp.in2p3.fr/preplapp/psexp/lappexp0002.ps.gz.
39. The LEP Collaborations, the LEP Electroweak Working Group and the SLD Heavy Flavour and Electroweak Groups, CERN–EP/2001-098, hep-ex/0112021.
40. N. De Groot *Electroweak results from SLD*, talk presented at XXXVIth Recontres de Moriond, Electroweak Interactions and Unified Theories, Les Arcs, March 2001, hep-ex/0105058; Serbo V. Presented at Int. Europhys. Conf. High Energy Phys., July 2001, Budapest, Hungary; SLD Collaboration, J. Brau, *"Electroweak Precision Measurements with Leptons"*, talk presented at EPS-HEP-99, Tampere, Finland, 15–21 July 1999.
41. UA2 Collaboration, J. Alitti *et al.*, Phys. Lett. **B276** (1992) 354.
42. CDF Collaboration, F. Abe *et al.*, Phys. Rev. Lett. **65** (1990) 2243 and Phys. Rev. **D43** (1991) 2070.
43. CDF Collaboration, F. Abe *et al.*, Phys. Rev. Lett. **75** (1995) 11 and Phys. Rev. **D52** (1995) 4784;
A. Goldon, talk presented at XXXIInd Rencontres de Moriond, Les Arcs, 16-22 March 1997, to appear in the proceedings.
44. DØ Collaboration, S. Abachi *et al.*, Phys. Rev. Lett. **84** (2000) 222.
45. http://www-cdf.fnal.gov/physics/ewk/wmass_new.html
46. CCFR/NuTeV Collaboration, K. McFarland *et al.*, Eur. Phys. J. **C1** (1998) 509.
47. NuTeV Collaboration, K. McFarland, talk presented at the XXXIIIth Recontres de Moriond, Les Arc, France, 15–21 March, 1998, hep-ex/9806013.
48. C. S. Wood *et al.*, Science **275** (1997) 1759.
49. S. C. Bennet and C. E. Wieman, Phys. Rev. Lett. **82** (1999) 2484 – 2487.
50. A. Derevianko, Phys. Rev. Lett. **85** (2000) 1618.
51. S. G. Porsev, M. G. Kozlov and I. I. Tupitsyn, Phys. Rev. Lett. **86** (2001) 3260.
52. CDF Collaboration, W. Yao, t Mass at CDF, talk presented at ICHEP98, Vancouver, B.C., Canada, 23-29 July 1998.
53. DØ Collaboration, B. Abbott, *et al.*, Phys. Rev. Lett. **84** (2000) 222.
54. The top Average Group, L. Demortier *et al.*, for the CDF and DØ Collaborations, FERMILAB-TM-2084 (1999).
55. T. van Ritbergen and R. G. Stuart, Phys. Rev. Lett. **82** (1999) 488.
56. K. Hoffman, *"Year 2000 update for OPAL and LEP HIGGSWG results"*, talk presented at ICHEP2000, Osaka, July 27 – August 2, 2000, to appear in the proceedings.
57. H. Burkhardt and B. Pietrzyk, Phys. Lett. **B513** (2001) 46.
58. A. D. Martin, J. Outhwaite and M. G. Ryskin, Phys. Lett. **B492** (2000) 69.